Quaternary Science Advances 17 (2025) 100266

Contents lists available at ScienceDirect

Quaternary Science Advances

journal homepage: www.sciencedirect.com/journal/quaternary-science-advances

Reconstruction of deep-water undercurrent variability from the outer Labrador Sea during the past 550,000 years

Stefanie Kaboth-Bahr [a,b,*], André Bahr [b], Patrick Blaser [c,d], Antje H.L. Voelker [e,f], Jörg Lippold [b], Marcus Gutjahr [d], David A. Hodell [g], James E.T. Channell [h], Anne de Vernal [i], Claude Hillaire-Marcel [i]

[a] Institute of Geological Sciences, Freie Universität Berlin, 12249, Berlin, Germany
[b] Institute of Earth Sciences, Heidelberg University, 69210, Heidelberg, Germany
[c] Institute of Earth Sciences, University of Lausanne, 1015, Lausanne, Switzerland
[d] GEOMAR Helmholtz Centre for Ocean Research Kiel, 24148, Kiel, Germany
[e] Divisao de Geologia e Georecursos Marinhos, Instituto Portugues do Mar e da Atmosfera (IPMA), 1495-165, Alges, Portugal
[f] Centro de Ciencias do Mar, Universidade do Algarve, 8005-139, Faro, Portugal
[g] Godwin Laboratory for Palaeoclimate Research, Department of Earth Sciences, University of Cambridge, Cambridge, United Kingdom
[h] Department of Geological Sciences, University of Florida, Gainesville, FL, 32611, USA
[i] Geotop Research Center, Université du Québec à Montréal, Montréal, CP 8888, Canada

A B S T R A C T

We present a comprehensive multi-proxy analysis spanning 550,000 years from the outer Labrador Sea region at the Integrated Ocean Drilling Program (IODP) Sites U1302/1303. We combine new benthic foraminiferal stable oxygen ($\delta^{18}O$) and carbon ($\delta^{13}C$) isotope records, with sediment elemental composition and authigenic neodymium isotope measurements, to provide insights into deep-water mass sourcing and changes of the Deep Western Boundary Current (DWBC), which exports North Atlantic Deep Water (NADW) into the wider North Atlantic as part of the lower limb of the Atlantic Meridional Overturning Circulation.

We find that a prominent DWBC likely remained a persistent feature within the Labrador Sea region throughout the past 550 kyr. However, glacial peaks of marine isotope stage (MIS) 14 to MIS 2 were consistently characterized by a weaker or shallower DWBC, while all interglacial periods of MIS 13a to MIS 1, with the exception of MIS 7e, were marked by enhanced DWBC. Additionally, the dominant deep-water masses feeding into the DWBC during these glacial-interglacial periods varied from regional (K-rich sediment, unradiogenic εNd) to more distal sources from the Nordic Seas (Ti-rich sediment, radiogenic εNd). Yet, these changes in deep-water provenance did not consistently correlate with DWBC strength, suggesting that additional factors may have played a significant role in shaping the DWBC strength or core depth throughout the geological past.

1. Introduction

The Atlantic Meridional Overturning Circulation (AMOC) plays an essential role in our climate system by meridionally exchanging of heat and salinity within the Atlantic Ocean, and worldwide (IPCC, 2021). Within its northward upper limb, the Gulf Stream and its northern extension, the North Atlantic Current (NAC), transport warm and salty waters to the northeast Atlantic, reaching the Nordic Seas in surface and subsurface waters (Fig. 1; Foukal and Lozier, 2016; Lozier et al., 2019). During winter time cooling heat is lost from the ocean to the atmosphere, which promotes deep mixing and convection of the North Atlantic waters across the Nordic, Irminger, and Labrador Seas (Fig. 1; Burkholder and Lozier, 2014; Lozier et al., 2013; Marshall and Schott, 1999). The newly formed North Atlantic Deep Water (NADW; see section 2 for more details) flows southward feeding the Deep Western Boundary Current (DWBC) (Fig. 1; Dickson and Brown, 1994; Molinari et al., 1998) and along isopycnals through interior cross-basin pathways, forming the lower limb of the AMOC (Bower et al., 2009; Foukal and Lozier, 2016; see section 2 for more details).

Because of its significance to Earth's climate, recent changes in AMOC strength have prompted substantial, albeit controversial, discussion about its future behaviour as a consequence of global climate change (e.g., Bryden et al., 2005; Caesar et al., 2021, 2018; Fu et al., 2020; Kilbourne et al., 2022). Past AMOC changes, in turn, are considered to have critically impacted the global ocean-atmosphere carbon dioxide (CO_2) exchange on glacial to interglacial time scales (Hasenfratz et al., 2019). The AMOC-modulated drawdown of atmospheric CO_2 (pCO_2) to the ocean and its re-release to the atmosphere have been

* Corresponding author.Institute of Geological Sciences, Freie Universität Berlin, 12249, Berlin, Germany
E-mail address: stefanie.kaboth-bahr@fu-berlin.de (S. Kaboth-Bahr).

https://doi.org/10.1016/j.qsa.2025.100266
Received 14 August 2024; Received in revised form 25 December 2024; Accepted 10 January 2025
Available online 13 January 2025

important for modulating the waning and waxing of large continental ice sheets during the Plio-Pleistocene (e.g., Chalk et al., 2017; Hasenfratz et al., 2019; Hönisch et al., 2009). In addition, deep-water convection in regions such as the Labrador Sea also act as "trapdoors" through which the oxygen ventilation of much of the deep ocean is facilitated (Atamanchuk et al., 2020).

To understand past AMOC variability – and thus to allow for a better assessment of its current and future behaviour - secular changes in the southward flow of NADW have been studied intensively, especially for modern-like interglacial conditions (Bouttes et al., 2020; Curry and Oppo, 2005; Galaasen et al., 2020; Howe and Piotrowski, 2017; Lynch-Stieglitz et al., 2007; Pena and Goldstein, 2014; Piotrowski et al., 2004; Yu et al., 2008). In contrast to its interglacial mode, the glacial AMOC was characterized by significant changes in the geometry of the North Atlantic surface and deep-water masses. During the Last Glacial Maximum (LGM; approx. 19–23 kyr), the ocean heat transport to the Nordic Seas was reduced (Rasmussen and Thomsen, 2004), likely affecting deep-water formation and resulting in the displacement of NADW to shallower depths (Gebbie, 2014; Oppo et al., 2018). In response, the underlying deep basins of the North Atlantic were filled with northward propagating southern sourced water masses (e.g., Böhm et al., 2015; Burckel et al., 2016; Curry and Oppo, 2005; Duplessy et al., 1988; Lippold et al., 2016; Sarnthein et al., 1994; Vidal et al., 1997). This conventional view of glacial AMOC variability has been challenged as new lines of evidence strongly argue for a persistent northern-sourced glacial NADW-analogue flowing south during the LGM (Blaser et al., 2020; Howe et al., 2016; Keigwin and Swift, 2017; Pöppelmeier et al., 2020, 2021; Seidenkrantz et al., 2021; Stevenard et al., 2024). However, it is yet to be determined what water mass configuration inferred for the LGM, based on distinct proxies such as $\delta^{13}C$, ^{14}C and εNd—each with its own advantages and limitations—was prevalent during earlier glacial periods of the Pleistocene.

This study provides constrains on past NADW changes within the DWBC region during peak glacial and interglacial background conditions of the past five climatic cycles (ca. 550 kyr). For this purpose, we studied sediment cores from the Integrated Ocean Drilling Program (IODP) Sites U1302 and U1303 (~3500 m water depth), situated in the core region of the DWBC in the outer Labrador Sea (Fig. 1). For

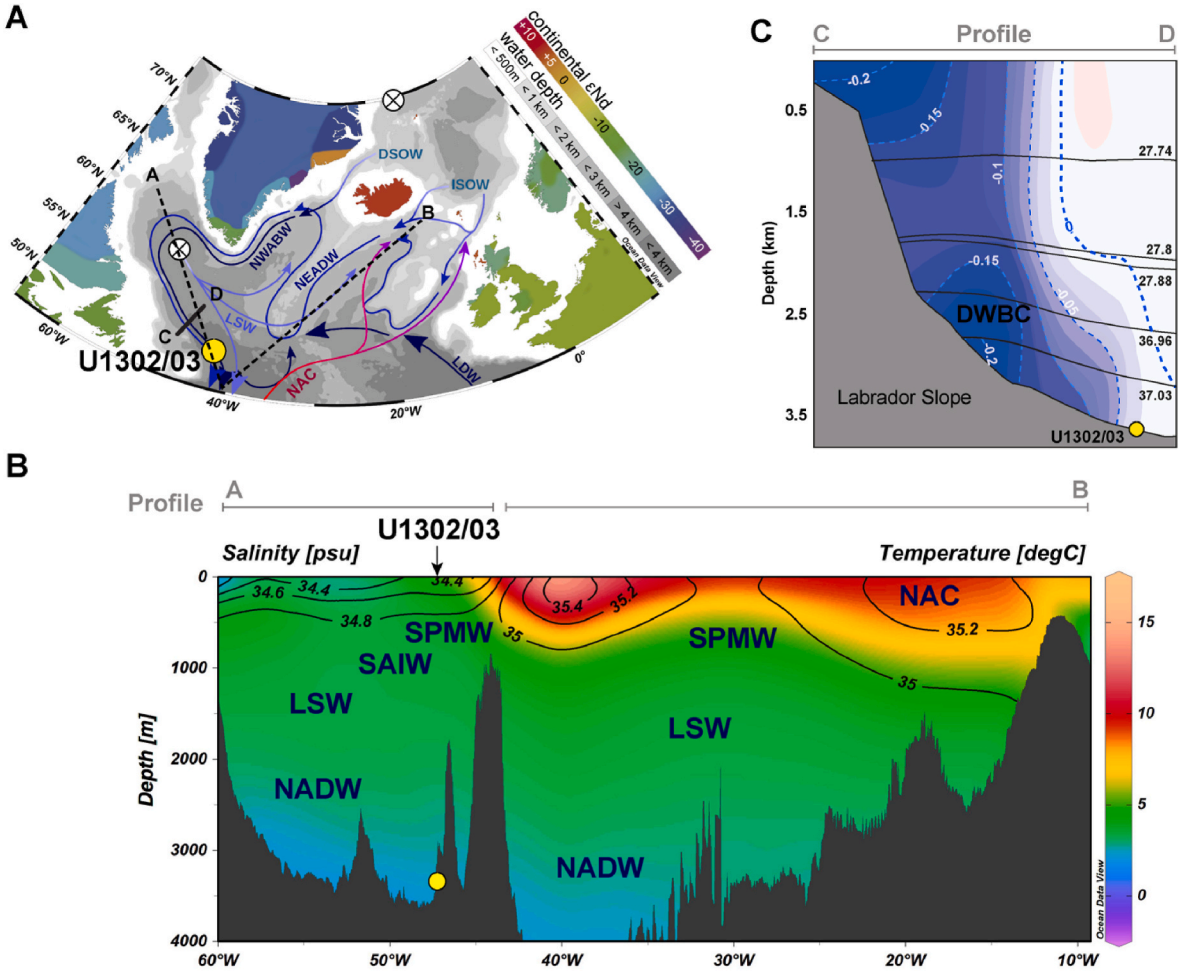

Fig. 1. Hydrography of the subpolar North Atlantic. (**A**) Schematic of dominant intermediate (bright blue arrows) and deep-water constituents (dark blue arrows) of the high-latitude North Atlantic deep-water regime. The location of Sites U1302/03 is marked by a yellow circle. NAC = North Atlantic Current; ISOW = Island-Scotland Overflow Water; DSOW = Denmark Strait Overflow Water; LSW = Labrador Sea Water; LDW = Lower Deep Water; NADW = North Atlantic Deep Water. Continental colours indicate their approximate bedrock neodymium isotope (εNd) compositions as estimated by Jeandel (2016). The grey-shaded bathymetric map was created with Ocean Data View (Schlitzer, 2002). Crossed circles approximately indicate regions of deep-water formation. Dotted black lines mark the position of the hydrographic profile from A to B shown in panel (B). The bold black line indicates flow velocity profile C to D shown in panel (C); (**B**) temperature (T) and salinity (Θ) profile across the western subpolar North Atlantic with added main water masses (Boyer et al., 2013; see section 2 for more details). SPMW = Subpolar Mode Water; SAIW = Subarctic Intermediate Water; (**C**) Mean velocity field along the 53°N profile C to D, computed from LADCP and mooring data (1997–2014) modified after Handmann et al. (2018). The mean velocity fields are superimposed by isotachs in m s−1 (white) and σ_2 and σ_0 mean isopycnals. Additionally, the 0 isotach is marked in dotted black. Blue velocities are directed to the southeast and red velocities are directed to the northwest. DWBC = Deep Western Boundary Current.

reconstruction of past NADW changes within the DWBC region, we utilized a suite of the commonly used proxies for deep-ocean circulation, including benthic foraminiferal stable oxygen ($\delta^{18}O$) and carbon ($\delta^{13}C$) isotopic records, authigenic neodymium (εNd) isotopes from bulk sediment leachates as well as the elemental compositions of the sediment. Our findings from Sites U1302 and U1303, complemented by data from earlier studies of these cores (e.g., Channell et al., 2012), are then placed into a regional context of existing intermediate and deep-water proxy records from the subpolar North Atlantic to document NADW geometry changes within the North Atlantic under peak interglacial and glacial conditions during the past ~ 550 kyr.

2. Modern physical circulation of the western north Atlantic

The NAC brings warm, salty waters into the northeast North Atlantic at surface and subsurface water levels (Fig. 1; Lozier et al., 2019). These waters circulate through the Norwegian and Greenland Seas, and gain density by heat loss to the atmosphere and winter deep mixing, forming Subpolar Mode Water (SPMW; Fig. 1). SPMW occupies the thermocline in an area bordered by Iceland in the north, the Reykjanes Ridge in the west, the Iceland-Faroe Ridge in the northeast, and the continental shelf of Great Britain in the east (Brambilla et al., 2008; Brambilla and Talley, 2008). Subpolar mode water is carried northward along the NAC to the Faroe Bank Channel, where it bifurcates with one branch providing warm SPMW to the Norwegian Current, and the other turning north-westward, eventually forming the Irminger Current (Fig. 1). Most of the Irminger Current recirculates south of the Denmark Strait flowing southward along the southern Greenland margin where it enters the Labrador Sea as the West Greenland Current, ultimately becoming part of the Labrador Current (Fig. 1; Pacini and Pickart, 2022).

Within the Nordic Seas, the SPMW also entrains cold fresh polar surface waters and other, denser, Arctic Ocean waters, that enter this region via the East Greenland Current through the Denmark Strait (Fig. 1; García-Ibáñez et al., 2015). Within the western North Atlantic, north of the Subpolar Front, SPMW is subducted to form Subarctic Intermediate Water (SAIW; Fig. 1).

The SAIW and SPMW in the western North Atlantic are underlain by the Labrador Sea water (LSW; Fig. 1) which results from modified SPMW in the Labrador Sea (McCartney and Talley, 1982) and contributes to the formation of various source water masses of NADW (Kawase and Sarmiento, 1986; Lee and Ellet, 1967; McCartney, 1992). The LSW is formed by deep convection in the centre of the Labrador Sea (e.g., Kieke et al., 2007; Lozier, 2010; Lozier et al., 2019; Marshall and Schott, 1999; Pickart et al., 2003). Depending on the strength of the winter-time atmospheric cooling over the Labrador Sea and local surface salinity/fresh water import, the convection region and depth of convection vary across time, with a thick and dense LSW layer forming in years of intense winter cooling (e.g., early to mid-1990s and around 2015/2016; up to 2500 m mixed layer depth; Lozier et al., 2019) while weaker convection resulted in less dense LSW vintages (Sy et al., 1997). In addition to warmer winter temperatures the influx of freshwater from melting Greenland and Arctic sources has been argued as a mechanism for decreased LSW convection after the mid-1990s, emphasizing the sensitivity of LSW production to freshwater forcing (Yang et al., 2016).

The export of LSW towards the eastern North Atlantic is facilitated along three primary pathways: (i) towards the south via the DWBC, (ii) eastward beneath and parallel to eastward flowing NAC, and (iii) north-eastward into the central Irminger Basin (Frew et al., 2000; Lozier et al., 2019). The eastward flowing LSW subsequently splits into a north-eastward component, entering the Iceland Basin and Rockall Trough (Fig. 1). However, the shallow sills of the Denmark Strait, Greenland-Scotland Ridge, and the Faroe Bank Channel prevent LSW from flowing directly into the Norwegian Sea. The speed of LSW, as it spreads across the North Atlantic, has been directly linked to its production rate as strong winter cooling is associated with a faster eastward spreading LSW (Sy et al., 1997). The LSW also interacts with two other water masses that constitute major parts of the NADW, i.e. the Iceland Scotland Overflow Water (ISOW) and the Denmark Strait Overflow Water (DSOW; Dickson and Brown, 1994; Tanhua et al., 2005). As the least dense of these three water masses, LSW feeds into upper NADW, underlain by the ISOW which provides central NADW, and the dense DSOW constitutes deep NADW (García-Ibáñez et al., 2015). Accordingly, the interaction of LSW is strongest with ISOW. However, intense mixing also occurs with DSOW as the latter contributes to the deepest waters in the Labrador Sea (Yashayaev et al., 2007).

3. Material and methods

3.1. IODP sites U1302 and U1303

IODP Site U1302 (50° 10 N, 45° 38 W, water depth: 3560 m) and Site U1303 (50° 12.4 N, 45°41.2 W, water depth: 3520 m) were drilled during IODP Expedition 303. The two sites are located 5.7 km apart off the Newfoundland continental margin on the SE flank of the Orphan Knoll and are bathed in NADW (Fig. 1; see section 2 for more details). They are positioned on a rise between two canyons that help to funnel turbidites and debris flows away from the sites (Channell et al., 2006) and situated well below the high-velocity core of the DWBC (Fig. 1; Mertens et al., 2014)). The sedimentary sequences at these two sites were found to be remarkably similar and were designated as a single site and subsequently spliced using shipboard multi-sensor track data following the IODP guidelines (Channell et al., 2006). The samples analysed herein follow the composite record expressed in meter composite depth (mcd; Channell et al., 2006). The investigated depth interval ranges from 0 to 77.75 mcd. In this interval, no debris flows (e.g., turbidites) are recorded at either site (Channell et al., 2006). Building on previously planktic foraminifera stable oxygen isotope ($\delta^{18}O_p$) and relative palaeointensity (RPI) based chronology (Hillaire-Marcel et al., 2011; Channell et al., 2012; see section 4 for more details), samples were investigated for benthic foraminifera at ~1 kyr resolution for the last ~ 550 kyr.

3.2. Stable oxygen ($\delta^{18}O$) and carbon ($\delta^{13}C$) isotope measurements

To assess the past deep-water changes in the stable oxygen and carbon isotope budget (reported as $\delta^{18}O_b$ and $\delta^{13}C_b$, respectively) we selected 3–8 specimens of either epifaunal benthic foraminifer species *Cibicidoides wuellerstorfi* or the shallow infaunal species *Hoeglundia elegans* and *Uvigerina peregrina* from the >106 μm grain-size fraction. The alternating use of these three species was necessary as none of the species was consistently present throughout the studied sediment interval (see Supplementary Fig. S1).

Time-successive changes in *C. wuellerstorfi* abundance in the North Atlantic have been linked to changes in the mode and magnitude of food supply from the surface waters (see Supplementary Fig. S1; Nees and Struck, 1999). Its low abundances during glacial periods are interpreted as resulting from changes in productivity linked to sea ice-edge fluctuations in the northern North Atlantic. There is a diametric increase in the abundance of the shallow infaunal *U. peregrina* during glacial stages relative to *C. wuellerstorfi*, which has been attributed to sluggish AMOC and lower organic matter fluxes (Schönfeld and Altenbach, 2005). The aragonitic species *H. elegans* was exclusively found during interglacial periods. The predominant presence of dissolution-prone *H. elegans* during interglacials at Site U1302/03 has been linked to the deepening of the lysocline under strong AMOC conditions (Gonzales et al., 2017; Streeter and Lavery, 1982).

Prior to measurement, the selected foraminifer tests were carefully crushed, ultrasonicated in methanol to physically remove contaminations (e.g., clays and nannofossils) and subsequently dried at 50 °C. The stable isotope measurements were carried out on a MicroMass Isoprime at the Geotop (Université du Québec à Montréal, UQAM, Montreal, Canada). The precision of the measurements is ±0.05 ‰ (one standard

deviation) for $\delta^{13}C$ and $\delta^{18}O$, respectively. The results were calibrated using the international standard NBS-19, and two in-house standards. Isotopic values are reported in standard delta notation (δ) relative to the Vienna Pee Dee Belemnite (VPDB).

Interspecies correction between the selected foraminifera follows Shackleton and Hall (1984) by applying a constant fractionation factor of +0.64 ‰ for $\delta^{18}O_b$ of *C. wuellerstorfi* and +0.9 ‰ for the $\delta^{13}C_b$ values of *U. peregrina*. *H. elegans* was corrected to equilibrium by applying a constant fractionation factor of −0.4 ‰ and 1.5 ‰ for $\delta^{18}O_b$ and $\delta^{13}C_b$, respectively (McCorkle et al., 1997). This was done to ensure comparability with existing deep and intermediate water $\delta^{13}C_b$ and $\delta^{18}O_b$ records from various locations in the North Atlantic which have been corrected using the same fractionation factors (Lisiecki and Raymo, 2005).

3.3. X-ray fluorescence scanning (XRF)

High-resolution (~1 cm interval) elemental composition data of sediments at Sites U1302/03 were obtained by non-destructive XRF core scanning at the University of Bremen using an Avaatech XRF core scanner. The instrumental settings for the XRF measurements are the same as those described by Hodell et al. (2008) and the resulting Ca/Sr and Si/Sr ratios were published previously by Channell et al. (2012). We normalized the raw total counts of a given element to the total counts of all processed elements, excluding silver (Ag) and rhodium (Rh) because these elements are biased by signal generation from the slit and X-ray tube, respectively. To eliminate non-linear matrix effects and constant-sum constraints we used log ratios following Weltje et al. (2015). For this study, we focused on two selected element ratios (K/Ti and Zr/Al) to gain insights into the spatiotemporal variability of the DWBC.

Firstly, we utilized the ln(K/Ti) ratio, which traces the contribution of Ti derived from the weathering of basaltic rocks found within the volcanic area including Iceland, the Faeroe Islands, and the eastern part of Greenland. K is predominantly derived from the weathering of the granite province of the Canadian Shield, Baffin Island, and western and southern Greenland (e.g., Ballini et al., 2006 and references therein). Within the broader region of the Labrador Sea and the Nordic Seas, the K/Ti ratio has been used as a tracer for deep-water mass provenance. Increased Ti concentrations within the Labrador Sea have been associated with periods of active DSOW or ISOW contributions to the DWBC, reflecting enhanced deep-water convection in the Nordic Seas (Ballini et al., 2006; Davies et al., 2021; Fagel et al., 1999, 1997, 1996; Grützner and Higgins, 2010; Hodell et al., 2010; Rashid et al., 2019; Stevenard et al., 2024; Yang and Piper, 2021).

Secondly, to understand the spatiotemporal variability of the DWBC strength, we employed the ln(Zr/Al) ratio. This ratio is suggested to trace relative changes between the coarser, more weathering-resistant Zr and the fine-grained clay-related Al (Hoffmann et al., 2019; Rashid et al., 2019). Zr is a dominant trace element of the Canadian Precambrian shield (Rashid et al., 2019), and is supplied to the Labrador Sea through riverine discharge. An increase in Zr relative to Al values in the ln(Zr/Al) ratio suggests sediment coarsening, and *vice versa* (Bahr et al., 2014; Nichols et al., 2020). However, this proxy has not yet been applied to the wider region of the Labrador Sea. To verify its applicability as a measure of grain-size variability and potential current strength activity at Site U1302/03, we compared the ln(Zr/Al) ratio with available sortable silt mean size ($\overline{SS}$) data (10–63 μm size fraction) from Site V23-18, located close to our study site in the outer Labrador Sea region, over the last ~20 kyr. (see Supplementary Information Fig. S2; Hoffmann et al., 2019). $\overline{SS}$ is a well-established proxy for grain-size variability in deep-water regimes (e.g., McCave et al., 2017, 1995; Praetorius et al., 2008; Thornalley et al., 2013).

The correlation (see section 3.5 for more details) between ln(Zr/Al) and $\overline{SS}$ is significantly positive ($r_{Spearman} = 0.40$; $p = 0.0075$). We propose that ln(Zr/Al) at Site U1302/03 serves as a proxy for grain-size variability controlled by bottom-current velocity.

3.4. Neodymium (εNd) measurements

Over the past decades, neodymium (Nd) isotopes emerged as a promising geochemical tracer of water mass provenance (e.g., Böhm et al., 2015; Piotrowski et al., 2004; Pöppelmeier et al., 2022). Because its radiogenic isotope composition is independent of environmental fractionation and recorded in marine sediments (Frank, 2002), Nd isotopes provide a valuable tool for assessing the origin of water masses and to reconstruct the physical state of the ocean in the past. However, along continental margins, isotopic exchange with glacially-derived sediment may impact original water-mass εNd-signatures (e.g., Böhm et al., 2015; Filippova et al., 2023; Lacan and Jeandel, 2005; Pöppelmeier et al., 2019; Zhao et al., 2019). Interpretation of exchangeable Nd-isotope records thus requires comparison with similar measurements of the bulk sediment detrital fraction.

We extracted the εNd isotope composition from a total of 84 samples by weak acid-reductive leaching of bulk sediment following the method described by Blaser et al. (2016). Briefly, 250–300 mg of dried and ground sediment were washed for 30 min with ultra-pure deionised water. After centrifugation the water was decanted and discarded. The authigenic fraction and carbonates were then leached with 10 ml of an acid-reductive aqueous solution containing 3 mM Na-EDTA, 5 mM hydroxylamine-hydrochloride, and 1.5% trace metal clean acetic acid buffered to a pH of 4 using trace metal clean 25% ammonia solution. After ~60 min of agitation the samples were centrifuged and pipetted for further analysis. However, recent εNd results by Blaser et al. (2020) have shown that detrital carbonate can affect the leaching efficiency of sediments from the Labrador Sea. Hence, for comparison a total of 48 samples across the studied time frame were decarbonated before subjecting them to the same leaching procedure as stated above. For carbonate removal, 10 ml of an acetic acid/sodium acetate buffer (NaAc/CaOH (ADA)) was applied to the dried and ground sediments for 30 min. Afterwards the samples were washed and rinsed three times with ultra-pure deionised water before proceeding with the leaching protocol following Blaser et al. (2016). The dual approach of analyzing decarbonate and non-decarbonated samples side-by-side allows for a direct comparison and assessment of potential detrital carbonate influences on the resulting εNd signals through time (see Fig. 4).

Subsequent to the leaching, the remaining sample solution was purified with a two-step column chemistry protocol for the measurements of Nd isotopes on a *Nu Instruments Plasma II* MC-ICP-MS at Geotop (UQAM) and a *Thermo Scientific Neptune Plus* MC-ICP-MS at the GEOMAR Helmholtz Centre for Ocean Research Kiel. Nd isotope data were corrected to $^{146}Nd/^{144}Nd$ of 0.7219 with an exponential law and normalized to JNdi-1 standards with $^{143}Nd/^{144}Nd = 0.512115$ (Tanaka et al., 2000). Reproducibility was assessed by repeated measurements of respective in-house standard solutions and varied in εNd from 0.12 to 0.63 (two standard deviations) between measurement sequences. The resulting uncertainty for εNd values is ~0.2 epsilon units (95% confidence).

3.5. Multivariate statistic

To assess the similarities between two different signals, the correlation coefficient and its significance using a bootstrap (Monte Carlo) procedure for serially correlated data were estimated using the 'surrogateCor' function as implemented in the *astrochron* package of R (Meyers, 2014). The correlation method was set to Spearman. For the simulation, 10,000 phase-randomized surrogate series were generated, and the significances of the correlation coefficients were tested at the 95 percentile. Utilized records were detrended prior to analysis as time-dependent trends suggest the expected value of the signal under study is non-stationary. However, stationarity is a fundamental

assumption for most of the data analysis algorithms such as cross-correlation (Box et al., 2015).

4. Chronology

The age model was established by visually correlating the composite $\delta^{18}O_b$ record of Site U1302/03 to the global benthic $\delta^{18}O$ compilation LR04 (Lisiecki and Raymo, 2005) assuming an in-phase behaviour of both signals. This approach is feasible as LR04 represents a globally averaged deep-water signal (Lisiecki and Raymo, 2005), and can thus be correlated to the deep-water signal recorded at Site U1302/03. The resulting $\delta^{18}O_b$ tuning is shown in Fig. 2 and the applied tie points are listed in Table 1. The assignment of Marine Isotope Stages (MIS) follows the chronology suggested by Lisiecki and Raymo (2005).

To test the robustness of our $\delta^{18}O_b$ tuning approach, we compared our tuning result to the previously established age model for Site U1302/03 (Channell et al., 2012) constructed by tandem fitting of $\delta^{18}O_p$ and relative paleointensity (RPI) to the LR04 benthic $\delta^{18}O$ stack (Lisiecki and Raymo, 2005) and the PISO-1500 RPI stack (Channell et al., 2009), respectively.

Interestingly, this comparison highlights distinct time-offsets ranging from 4 up to 10 kyr during the climate terminations TI-TIII,

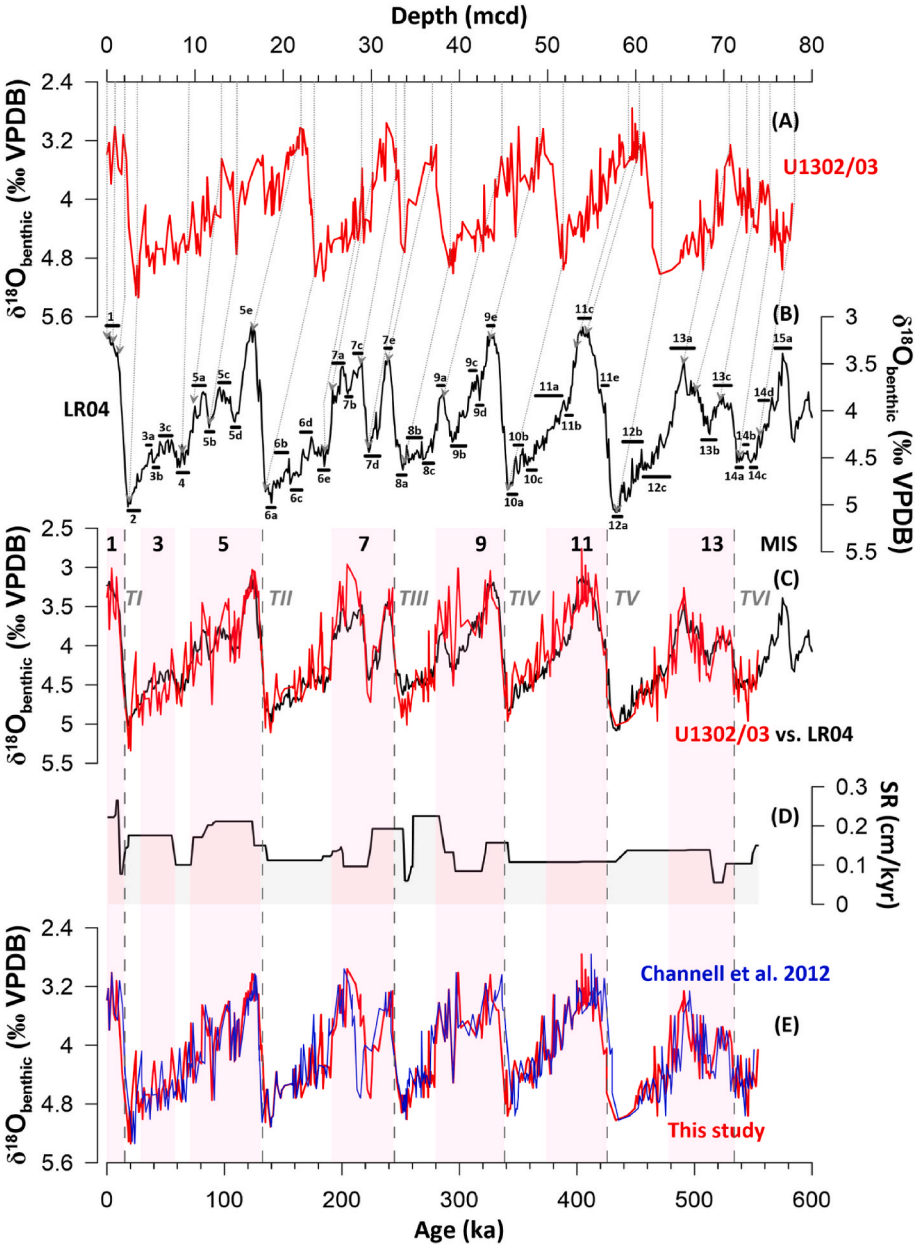

Fig. 2. Chronostratigraphy of Site U1302/03. Assignment of Marine Isotope stages (MIS), their individual substages and terminations (T) follows Lisiecki and Raymo (2005); (**A**) composite benthic stable oxygen isotope ($\delta^{18}O_b$) record of Site U1302/03 in the depth domain (meter composite depth; mcd; red line); (**B**) reference global benthic $\delta^{18}O$ compilation LR04 used as tuning target in the time domain (black line; Lisiecki and Raymo, 2005) for the last ~ 550 kyrs (black line). Age-depth tie points utilized for the tuning are indicated by grey arrows and are listed in Table 1; (**C**) comparison of the temporal fit between the tuned composite benthic stable oxygen isotope ($\delta^{18}O$) record of Site U1302/03 (red line) and the reference global benthic $\delta^{18}O$ compilation LR04 record (black line) in the time domain; (**D**) Resulting Sedimentation rate (SR) in cm/kyr during the past ~550 kyr, and (**E**) Comparison of the composite benthic stable oxygen isotope ($\delta^{18}O_b$) record of Site U1302/03 based on the tuning proposed in this study (red line; see section 4 for more details) and the Site U1302/03 age model proposed by Channell et al. (2012) (blue line) based on the tandem alignment relative palaeointensity (RPI) record with a calibrated RPI template (Channell et al., 2014) and the planktic stable oxygen isotope ($\delta^{18}O_p$) record from Site U1302/03 (Hillaire-Marcel et al., 2011) to the LR04 reference signal (Lippold et al., 2019).

Table 1
Age-depth tie points derived from the visual correlation of the composite benthic stable oxygen isotope ($\delta^{18}O_b$) record of Site U1302/03 to the global benthic $\delta^{18}O$ compilation LR04 (Fig. 2; see section 4 for more details; Lisiecki and Raymo, 2005). mcd = meter composite depth.

Depth (mcd)	Age (ka)
0	0
1.6	7
2.21	10
2.48	13
3.2	18
9.73	55
11.38	72
13.01	81
14.81	90
22	124
23.65	135
29.01	183
30.01	191
30.81	197
31.31	200
33.5	223
39.09	252
39.39	257
39.69	260
44.75	283
46.36	295
48.5	320
51.8	341
58.15	400
59.6	404
62.76	433
70.74	491
73.79	513
74.4	524
77	549
78.8	561

-TIIIa between at 204–236 kyr (MIS7d/c) and TV (Fig. 2). Thus, to investigate the origin of these temporal offsets, we directly compared the planktic and benthic $\delta^{18}O$ signal in the depth-domain for terminations TI-TVI alongside the ln(Ca/Sr) ratio indicating ice-rafted debris (IRD) rich in detrital carbonate (Fig. 3). Utilizing the proposed 3.5 ‰ threshold in $\delta^{18}O_b$ as a visual cut-off value for the mid-point of the climate transitions (McManus et al., 1999), we find that the decrease in the $\delta^{18}O_p$ precedes the decrease in $\delta^{18}O_b$ particularly during TI-III, most profoundly at TIIIa and TV. TIV and TVI cannot be properly assessed due the low sample resolution in both planktic and benthic $\delta^{18}O$ signals (TIV) as well as the fact that the $\delta^{18}O_b$ data does not reach the 3.5 ‰ threshold (TVI), respectively.

The earlier onset of decrease in the planktic $\delta^{18}O$, relative to the $\delta^{18}O_b$ signal, along transitions TI-III, TV and at TIIIa generally aligns with increased IRD riched in detrital carbonate as marked by high ln(Ca/Sr) ratios (Fig. 3). This relationship indicates that the temporal offsets between benthic and planktic $\delta^{18}O$ stems from freshwater influx, as increased IRD concentrations are generally thought to coincide with freshwater release from melting icebergs. In this scenario, freshwater with low $\delta^{18}O$ mixed with surface water but did not penetrate to the bottom water regime at Site U1302/03. This would have caused a decrease in the $\delta^{18}O_p$ signal relative to the freshwater-unaffected deep-water $\delta^{18}O_b$ signal. Previous tandem (equal weight) correlations for $\delta^{18}Op$ and relative palaeointensity (RPI) also implied meltwater influence during terminations at Site U1302/03 (Channell et al., 2012) and at Site U1306 on the Eirik Drift (Channell et al., 2014). Freshwater pulses coinciding with TI-IIIb and TIIIa have been documented in the central Arctic Ocean (Spielhagen, 2004) and northern Fram Strait (Knies et al., 1998; Vogt and Knies, 2008). The latter constitutes today an important source region for freshwater entering the Labrador Sea via the East Greenland Current (Yang et al., 2016). It is also possible that regional freshwater input from southern Greenland, the Hudson Bay and the Canadian Arctic Archipelago occurred during these transitions which contributed to $\delta^{18}O_p$ decreases relative to the deep-water signal at Site U1302/03. However, freshwater pulses from these regions throughout the last ~550 kyr are not well recorded. Thus, direct insights into potential freshwater pulses along the older terminations are hampered.

Our age model results in sedimentation rates ranging between 5 and 25 cm/kyr (Fig. 2). The sedimentation rates are generally higher during interglacial stages (e.g., MIS 5e) than glacial periods, with the exception of MIS 8. The median sedimentation rate is ~10 cm/kyr.

5. Results

5.1. Benthic stable oxygen and carbon isotopes at site U1302/03

The composite $\delta^{18}O_b$ values range from 2.7 ‰ to 5.3 ‰ throughout the last ~550 kyr (Fig. 4). The lowest values were observed in MIS 1, 5e, 7a, 7c, 7e, 9e, 11c and 13a with a range between 2.7 ‰ (MIS 11c) and 3.7 ‰ (MIS 1). In contrast, increases in $\delta^{18}O$ occurred during MIS 2, 4, 6, 8, 10, 12 and 14, ranging from 3.6 ‰ (MIS 6e) to 5.3‰ (MIS 2).

The composite $\delta^{13}C_b$ values range from −0.4 ‰ to 1.6 ‰ throughout the last ~550 kyr (Fig. 4). The lowest $\delta^{13}C_b$ values (0 to −0.4‰) align with MIS 6, 8, 10, and 12. In contrast, the highest $\delta^{13}C_b$ values coincide with MIS 1, 5e, 7a, 7c, 7e, 9a, 9c, 11c and 13a ranging from 1.65 ‰ (MIS 13a) to 0.4 ‰ (MIS 7a).

5.2. ln(K/Ti) ratio and ln(Zr/Al) ratio

The ln(K/Ti) ratio varies between 0.63 and −0.41 throughout the last ~550 kyrs (Fig. 4). Increased ln(K/Ti) values are associated with MIS 5 (particularly MIS 5e), 6c-6e, 10 and 13 but also transitional periods such as MIS 12/11, 10/9 and 6/7. In contrast, decreased ln(K/Ti) values are associated with MIS 2–4, 6a to c, 8a, 11c, and 12.

The ln(Zr/Al) ratio varies between 0.93 and −1.14 throughout the last ~550 kyrs (Fig. 4). Increased ln(Zr/Al) values are predominantly observed during MIS 2, 6, 8, 10, and 12 but also are concurrent during MIS 7e. Decreased ln(Zr/Al) values are associated with MIS1, (including 5e), 9 (including 9e), 11 (including 11c) and 13 (including 13a).

5.3. εNd results

The median analytical error for "weak leach" (n = 73) and "weak leach + pre-decarbonization" samples (n = 32) is ±0.2 εNd, respectively. Furthermore, the median precision based on replicates (n = 6) is ±0.5 εNd for both approaches, and the median standard deviation between "weak leach" and "weak leach + pre-decarbonization" samples for the same time interval (double measurements within ~300-year time windows; n = 23) is 1.6 εNd.

The average εNd value across the past ~550 kyr (Fig. 4) is −19 and ranges between −29 (at ~94 ka) and −11 (at ~54 ka). Very unradiogenic Nd isotope compositions (low εNd) can be observed during MIS4 (−24 ± 4), peak MIS 10 (−20 ± 1), peak MIS 14 (−20 ± 2) as well as MIS 5 (−21 ± 2), MIS 7a-c (−20 ± 5), MIS 9e (−21 ± 3) and MIS 13a (−20 ± 6). In contrast, more radiogenic Nd isotope compositions (high εNd) prevailed during MIS 1 (−16 ± 2), MIS 2 (−17 ± 2), peak MIS 6 (−16 ± 3), peak MIS 8 (−15 ± 0.5), MIS 11c (−16 ± 1) and peak MIS 12 (−17 ± 1).

6. Discussion

6.1. Late Pleistocene (past ca. 140,000 years) deep-water variability in the outer Labrador Sea

The most striking aspect of our εNd record spanning the past ~140 kyr is its distinct two-phased behavior (Fig. 5). We observe a progressive

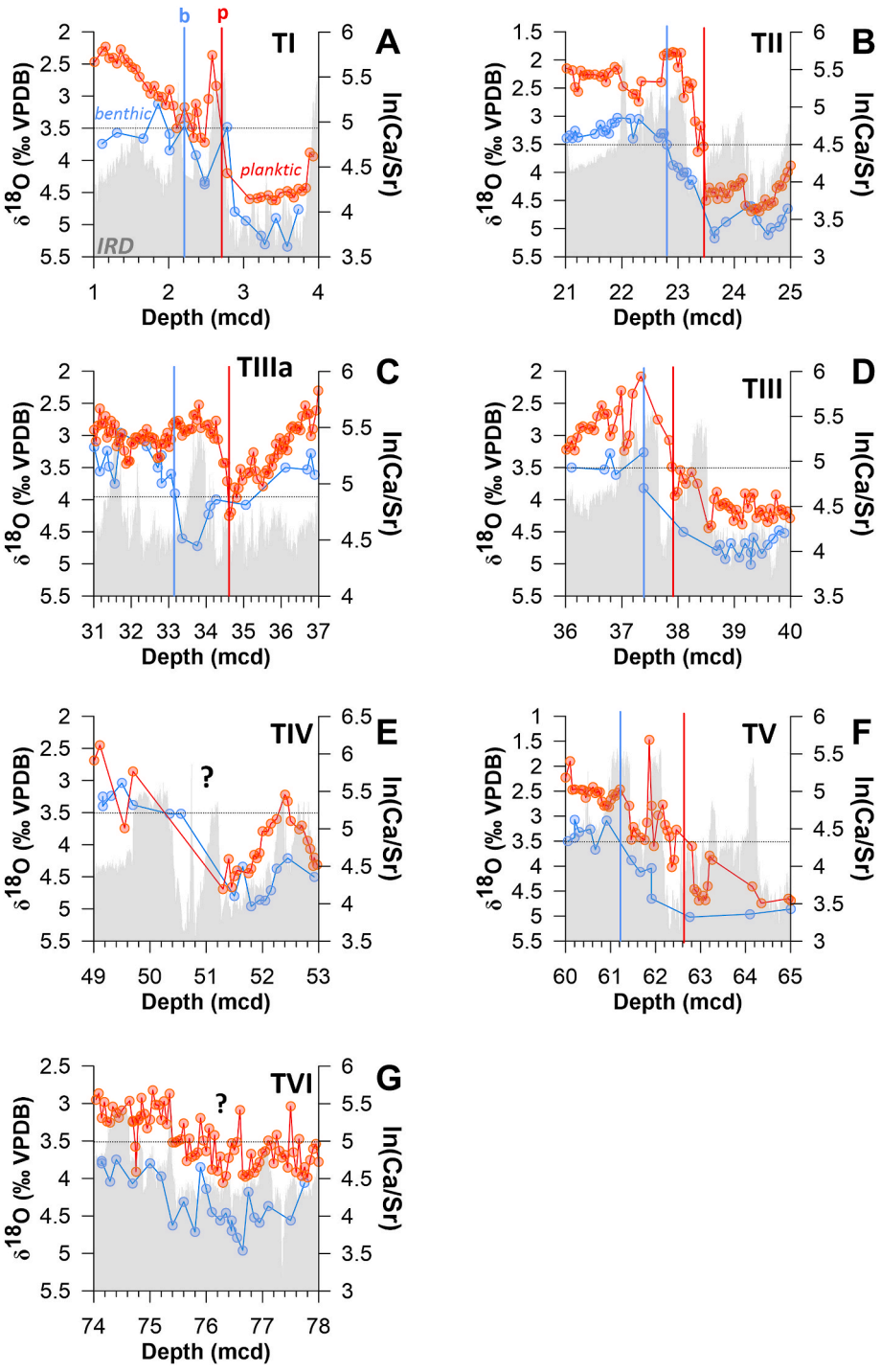

Fig. 3. Comparison between planktic (red line) and benthic stable oxygen isotope ($\delta^{18}O$) (blue line) in the depth domain (meter composite depth, mcd; this study) for climate transitions (**A-G**) during the past ~550 kyr at Site U1302/03. In addition, the ln(Ca/Sr) ratio is shown as a grey-shaded area tracing ice-rafted debris (IRD) influx (Channell et al., 2009). Assignment of climate terminations (TI-VI) follows Lisiecki and Raymo (2005) while the assignment of TIIIa follows Hodell et al. (2023). The proposed 3.5 ‰ threshold in benthic $\delta^{18}O$, as a visual cut-off value for the mid-point of the climate transitions (McManus et al., 1999), is indicated as a grey line. The intercepts with the planktic and benthic $\delta^{18}O$ records with the 3.5 ‰ threshold are indicated by vertical red (planktic = p) and blue (benthic = b) vertical lines.

shift from a strongly unradiogenic background state during MIS 5 (median: −22 εNd) to more radiogenic values during MIS 3 to 1 (median: −17 εNd), following a rapid increase of ~5 εNd at the end of MIS 4 (~70 kyr). For comparison, modern Labrador Sea εNd values range from −16.8 to −14.9 (±2) at the surface, becoming more radiogenic at the bottom, ranging from −11 to −14 (±1.7), reflecting mixing of DSOW with NEADW (Filippova et al., 2017; Blaser et al., 2020). Within this context, εNd values from Site U1302/03 during MIS 3 to 1 align, within analytical uncertainty, with modern NADW signatures, while MIS 5 values suggest a distinctly more unradiogenic source during that interval. This long-term εNd evolution also appears unaffected by the applied neodymium leaching protocol, as samples processed using both the "weak leach" and "weak leach + pre-decarbonization" methods show the same trend (Fig. 5). Additionally, the observed background shift cannot

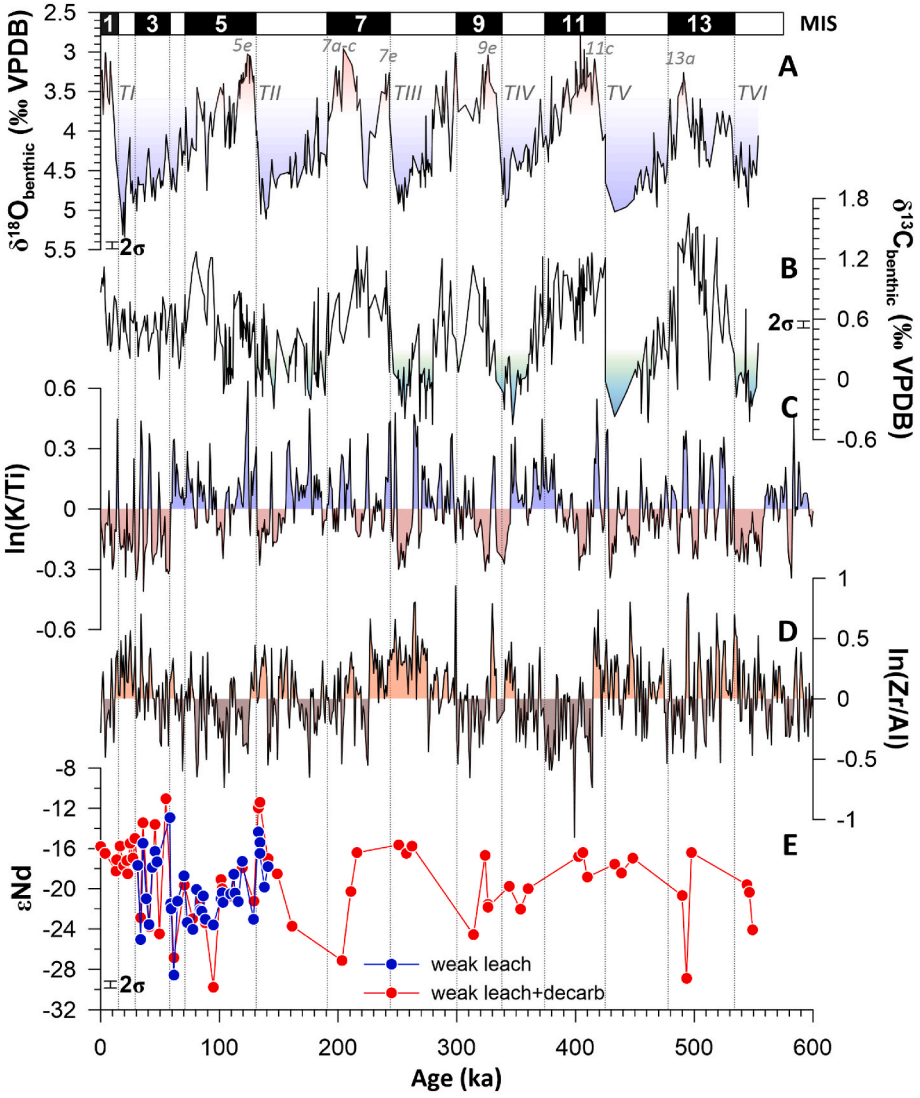

Fig. 4. Overview of the geochemical study results from Site U1302/03. (**A**) composite benthic stable oxygen isotope ($\delta^{18}O_b$) record; (**B**) composite benthic stable carbon isotope ($\delta^{13}C$) record; (**C**) detrended ln(K/Ti) ratio; (**D**) detrended ln(Zr/Al) ratio, and (**E**) composite εNd isotope record. All data is placed on the stable oxygen isotope ($\delta^{18}O$) tuning applied in this study (Fig. 2; see section 4 for more details). Assignment of Marine Isotope stages (MIS) follows Lisiecki and Raymo (2005).

be attributed to analytical uncertainty (see section 5.3 for more details).

Recent studies by Blaser et al. (2020) and Filippova et al., 2017 suggest that the bottom water εNd signal at our study site can be heavily overprinted by ice-rafted debris (IRD) input as shown during the Early Holocene, as well as during Heinrich Events (H) H1 and H2 (Blaser et al., 2020; Filippova et al., 2023). In general, IRD-hosts highly unradiogenic neodymium isotope signatures which are then released into the pore water and subsequently incorporated into the authigenic phases, shifting the εNd patterns towards substantially less radiogenic detrital signatures (Fig. 1; Blaser et al., 2020; Haley et al., 2017; Pöppelmeier et al., 2019, 2022). Thus, the strong millennial-scale unradiogenic excursions (~−20 to −28 εNd) we find associated with and H6 to H3 (Fig. 5) are in line with these earlier findings from H1 and H2. However, this raises the question of whether the long-term εNd shift might also be biased by this process.

To assess if this long-term εNd trend from unradiogenic MIS 5 sediments towards substantially more radiogenic MIS 3 to 1 values also relates to long-term IRD input, we utilized the XRF scanning-based Ca/Sr and Si/Sr ratios from our study site, which have been argued to trace carbonate and silicate IRD input, respectively (Fig. 5; Channell et al., 2012). We find that the Ca/Sr and Si/Sr levels between MIS 5 and MIS3 to 1 were, for the most part, comparable, after excluding Heinrich Events (Fig. 5). This suggests that no discernible long-term trend in IRD background supply accompanied our observed εNd trend from MIS 5 to MIS3 to 1. This disconnect is further supported by our Monte Carlo-based correlation results, which highlight only a weak correlation between Ca/Sr and Si/Sr in relation to εNd (see Supplementary Information Fig. S3). Hence, the discrepancy between the more radiogenic εNd signature of MIS 3 to 1 relative to the more unradiogenic signatures during MIS 5 should not predominantly relate to background changes in carbonate or silicate IRD input to our study site.

However, several studies have shown that an elevated benthic neodymium flux still occurs at our location unrelated to IRD events (Blaser et al., 2020; Pöppelmeier et al., 2022) and is instead driven by (i) weathering input variability linked to continental ice sheet geometry changes on glacial-interglacial time scales; and/or, (ii) reversed scavenging (Howe et al., 2016; Pöppelmeier et al., 2022). In terms of weathering input variability, a recent study of $^{206}Pb/^{204}Pb$ isotopes from our study site (Parker et al., 2022) found similar features during the past ca.140 kyr as observed in our εNd record (Fig. 5). The authors identified a shift from a predominantly radiogenic lead background state during MIS 5 to a less radiogenic background level from MIS 3 to 1. This was

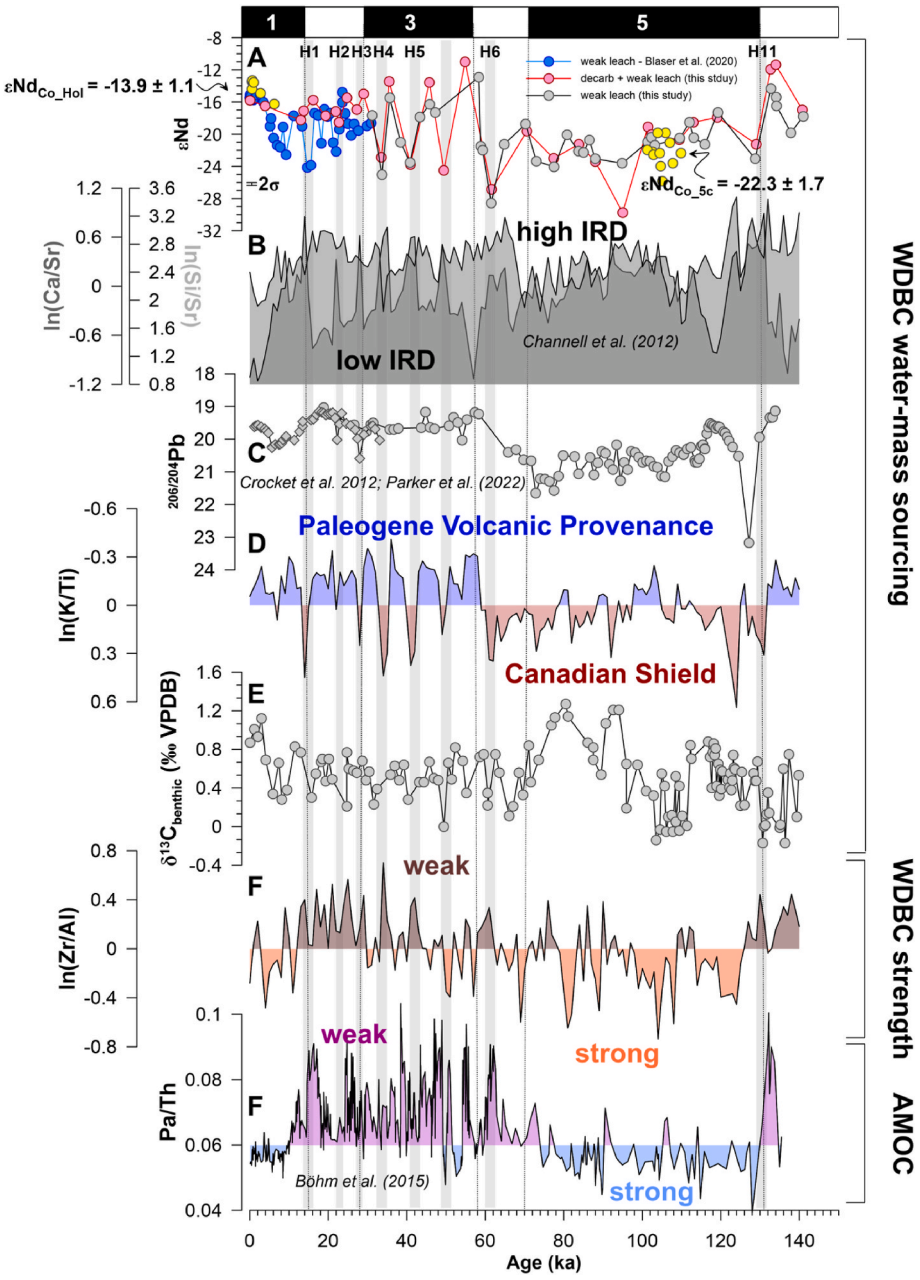

Fig. 5. Deep-water changes at Site U1302/03 during the past ~140 kyr. (**A**) composite neodymium isotope (εNd) isotope record of Site U1302/03 based on this study and data published in Blaser et al. (2020) for the time interval (0–35 kyr). Yellow stars denote modern εNd of the North Atlantic Deep Water (NADW; Blaser et al., 2020) as well as εNd signature of a cold water coral *Desmophyllum dianthus* (yellow dots) from Orphan Knoll for MIS 1 and MIS 5c (Maccali et al., 2020); (**B**) detrended and linearly resampled (~1 kyr step size) ln(Ca/Sr) and ln(Si/Sr) ratio at Site U1302/03 (Channell et al., 2012); (**C**) Published $^{204/206}$Pb isotope data from Sites U1302/03 (grey diamonds = Crocket et al., 2012; grey dots = Parker et al., 2022). Original age models of both data sets were adjusted to the tuning presented herein (see section 4 for more details); (**D**) detrended and linearly resampled (~1 kyr step size) ln(K/Ti) ratio at Site U1302/03 (this study); (**E**) composite benthic stable carbon isotope ($\delta^{13}C_b$) record at Site U1302/03 (this study); (**F**) detrended and linearly resampled (~1 kyr step size) ln(Zr/Al) ratio at Site U1302/03 (this study); (**G**) Pa/Th record of ODP 1063 (Bermuda Rise; 33°N 41.11'; 57°W 36.53'; 4500 m water depth; Böhm et al., 2015). Assignment of Marine Isotope stages (MIS) follows Lisiecki and Raymo (2005).

related to a mixture of (i) weathering input changes due to ice sheet dynamics on the adjacent continents, and (ii) changes in the vigour of the prevailing deep-water circulation (Parker et al., 2022).

Specifically, Parker et al. (2022) suggested that during MIS 5 a vigorous Labrador Current supplied more radiogenic ^{206}Pb/^{204}Pb isotopes from the inner Labrador Sea to the Orphan Knoll region. The continued re-supply of radiogenic ^{206}Pb/^{204}Pb from the Labrador/Quebec Superior province during MIS 5, in turn, was facilitated by renewed glacial erosion and chemical weathering during the incipient MIS 5 glaciations (MIS 5d and 5b), with subsequent outwash into the interior Labrador Sea during the following interstadial phases (MIS 5c and 5a). The observed rapid isotopic shift during MIS 4/3 transitions towards less distinctive NW Atlantic unradiogenic ^{206}Pb/^{204}Pb isotope values, which continued onwards between MIS 3 and 1, was subsequently related to an interplay of several factors, including (i) reduced weathering input due to Laurentide Ice Sheet advances across the Hudson Bay and Superior province regions; (ii) a less vigorous Labrador Current associated with a reduced detrital transport from the inner to the outer Labrador Sea; and, (iii) an increased input of unradiogenic ^{206}Pb/^{204}Pb of southern Greenland Provenance that might have

experienced temporal ice-free conditions allowing for chemical weathering and detrital supply to the Labrador Sea especially during MIS 3 (Parker et al., 2022).

Thus, as a next step, we tested these $^{206}Pb/^{204}Pb$ isotope-based scenarios against our εNd and K/Ti signals. Firstly, we focus on MIS 5. Detrital material from the inner Labrador Sea carries a distinct unradiogenic εNd signal, as the material is predominantly sourced from old cratonic provenances surrounding the Labrador Sea, which exhibit strong unradiogenic signatures ranging from −47 εNd (Nain Provenance) to −28 εNd (Superior Provenance). Therefore, a stronger supply of detrital material into the inner Labrador Sea and/or an increased export of detrital material from the inner Labrador Sea to our study site via the Labrador Current during MIS 5 relative to MIS 3 to 1 would align with the observed εNd differences. This scenario is also supported by the observed high K/Ti ratio values during MIS 5 relative to the period MIS 3 to 1 (Fig. 5; see section 3.3 for more details). Previous studies have shown that physical erosion and/or moderate chemical weathering of the Canadian Shield, Baffin Island, as well as western and southern Greenland produces a mineralogy characterized by K-rich illite and chlorite (Ballini et al., 2006; Biscaye, 1965; Fagel et al., 1996, 1997, 1999, 2001; Griffin et al., 1968). Hence, the high K/Ti values during MIS 5 support a dominant Hudson Bay-Superior Provenance terrane region for the detrital material deposited at our study site at that time.

In the previously proposed MIS 3 scenario, the reduction of unradiogenic εNd detrital input into the inner Labrador Sea due to ice sheet advances and/or the reduction of transport of unradiogenic detrital material from the inner to the outer Labrador Sea (Parker et al., 2022) could both facilitate a shift in εNd towards less radiogenic values, aligning with our data. Similarly, the proposed shift towards a South Greenland Margin Provenance with more radiogenic εNd signature (Fig. 1; median value: −18 εNd; Blaser et al., 2020) than the strong unradiogenic Nain-Superior provenances (Parker et al., 2022) could also have led to more radiogenic εNd values as shown in our data. However, our low K/Ti ratios between MIS 3 to 1 relative to MIS 5 might point towards a different scenario altogether. Neither of the aforementioned provenances nor the Orphan Knoll region itself is a prominent source for Ti (Ballini et al., 2006; Biscaye, 1965; Fagel et al., 1996, 1997, 1999, 2001; Griffin et al., 1968; Zimmermann, 1982). Hence, a reduction in the supply of K-rich detrital material from the inner Labrador Sea and/or a shift from the K-rich inner Labrador Sea detritus to the K-rich southern Greenland margin detritus would not necessarily explain increased Ti contributions.

Thus, we argue that the shift in K/Ti indicates increased supply of Ti-rich detrital material to our study site. Ti-rich weathering products have been distinctly linked to the volcanic areas comprising Iceland, the Faeroe Islands, and the eastern part of Greenland (Paleogene Volcanic Provenance). These regions are all dominated by Tertiary and Quaternary basaltic rocks that are rich in magnetite (Grousset et al., 1982; Kissel et al., 1999; Lackschewitz et al., 1994; Lavrov et al., 1971; Parra et al., 1986; Watkins and Maher, 2003). The physical and chemical weathering of magnetite results in Ti-rich smectites (Ballini et al., 2006; Biscaye, 1965; Fagel et al., 2001) that reach maximum concentrations in the submarine regions surrounding Iceland and the Faeroe-Shetland islands (Grousset et al., 1982; Parra et al., 1986). Hence, the shift in K/Ti from MIS 5 to MIS 3 to 1 likely indicates an increased supply of Ti-rich smectites which were transported from the subpolar North Atlantic via resuspension by the DSOW and ISOW onwards via the Eirik Drift into the Labrador Sea (Ballini et al., 2006; Davies et al., 2021; Fagel et al., 1997, 1996; Grützner and Higgins, 2010; Stevenard et al., 2024). A greater contribution of DSOW and ISOW to the DWBC during MIS 3 to 1 relative to MIS 5 could also explain the observed shifts in εNd and $^{206}Pb/^{204}Pb$ isotope values, respectively. Modern and glacial DSOW and ISOW derivatives have been shown to carry more radiogenic εNd signatures (−8 to −12 εNd; Fig. 1; Blaser et al., 2020; Struve et al., 2019). A greater import of these radiogenic waters into the DWBC would cause an εNd shift towards more radiogenic values at our study site. Additionally, the $^{206}Pb/^{204}Pb$ isotope signature of Paleogene Volcanic Provenance of the eastern flanks of Greenland are similarly unradiogenic as its southern margin counterparts. Hence, instead of increased input of unradiogenic $^{206}Pb/^{204}Pb$ from the southern Greenland provenance as previously proposed, perhaps temporal ice-free conditions during MIS 3 and 2 along Greenland's eastern flank allowed for chemical weathering in that region and increased supply of unradiogenic $^{206}Pb/^{204}Pb$, radiogenic εNd and high-Ti detritus to the Labrador Sea via DSOW and ISOW.

Based on the observed close relationship between εNd and K/Ti across the past 140 kyr, it becomes clear that our εNd likely carries a distinct signal driven by both sediment and deep-water provenance changes. This argument is supported by the comparison of our εNd leachates to available cold-water coral-based εNd originating directly from the Orphan Knoll (Fig. 5). These εNd results are derived from solitary stony coral *Desmophyllum dianthus* at ca. 1700 m water depth (Hillaire-Marcel et al., 2022; Maccali et al., 2020). The available coral data cover two distinct time periods, dating to the middle to late Holocene (ca. 1–6 kyr) and MIS 5c (ca. 102–109 kyr; Fig. 5; Maccali et al., 2020). These hardground coral εNd data are considered a robust recorder of the bottom water signature at the time (e.g., Struve et al., 2017). The coral-based median εNd values for the Holocene (εNd: −13.9 ± 1.1) and MIS 5c (εNd: −22.3 ± 1.7) (Hillaire-Marcel et al., 2022), agree with our leachate median values for the same periods (Fig. 5; midde to late Holocene εNd: −15.7 ± 1.7; MIS 5c εNd: −20.5 ± 0.4). This further supports the notion that the observed long-term shift in εNd reflects at least to some extent a direct bottom water neodymium isotope signature of the DWBC over the past ca. 140 kyrs. This finding is in agreement with previous research results by Blaser et al. (2020), arguing that the εNd signal 'outside' of distinct IRD events reflects bottom water conditions at our study site.

Based on the discussion presented above, our findings provide valuable insights into the dynamics of deep-water circulation within the Labrador Sea over the past 140 kyr. Specifically, during MIS 5, we propose a close association between deep-water circulation in the outer Labrador Sea and Labrador Current activity, consistent with the assertions of Parker et al. (2022). This linkage suggests a regional deep-water formation process driving Labrador Current activity. Given a suppression of LSW during MIS 5 (Hillaire-Marcel et al., 2001), we hypothesize that increased overflow of relatively dense waters from Baffin Bay through the Davis Strait may have contributed to the Labrador Current's intensification during this period, potentially influencing deep-water circulation patterns in the region. The Baffin Bay region would also be expected to yield very unradiogenic Nd isotope signatures (Stordal and Wasserburg, 1986). Additionally, we posit that during MIS 5, overflow water masses originating from distal sources, such as Paleogene Volcanic Province, appear to have had minimal influence on the deep-water circulation dynamics of the outer Labrador Sea and/or that their signal was overprinted by regional sources. However, during MIS 4 and transition MIS4/3, a notable and rapid transition occurred in the deep-water regime of the Labrador Sea, resulting in a circulation pattern predominantly influenced by distally-sourced deep-water production, including DSOW and/or ISOW - a pattern that has persisted into the modern era. This shift in deep-water production may have been driven by increased brine export from the Nordic Seas, as Thornalley et al. (2010) suggested.

However, this raises the question of whether these provenance changes in deep-water sourcing also translated into DWBC current strength changes and, by extension, variability in bottom-water ventilation in the western North Atlantic. To gain insights into DWBC strength changes, we utilize the Zr/Al proxy (Fig. 5; see section 3.3 for more details). Site U1302/03 is presently located well below the high-velocity core of the DWBC (Fig. 1), allowing fine sediments winnowed upslope by the current to accumulate preferentially at the site (Mertens et al., 2014). This is reflected in the low modern Zr/Al values observed at our site (Fig. 5), indicating fine sediment deposition beneath the DWBC.

Similar patterns of fine-grained sediment accumulation beneath the DWBC's path have been documented at the Eirik Drift off southern Greenland (Hunter et al., 2007). We thus argue that a shift to coarser sediment at Site U1302/03 indicates (i) a larger vertical distance of the study site from the DWBC flow core, leading to reduced fine-sediment resupply as the DWBC migrates to shallower depths. Therefore, we posit that the fining and coarsening of sediments at U1302/03 could serve as indicators of DWBC position and associated strength changes.

Such a scenario is supported by the significant correlation between Zr/Al and the Pa/Th ratio of ODP Site 1063 providing a record for AMOC strength variability in the western North Atlantic over the past 140 kyr (Fig. 5; Böhm et al., 2015; see Supplementary Fig. S3). We find that stronger AMOC phases are associated with finer sediment supply to Sites U1302/03 (MIS 5 and 1), while weaker AMOC phases are associated with coarser sediment deposition (MIS 4-2), possibly indicating phases of shallowed or weakened DWBC position during glacial stages (Fig. 5). A weaker DWBC during glacial stages has been argued to be a persistent feature since the Miocene (Müller-Michaelis and Uenzelmann-Neben, 2014). At Sites U1302/03, we also observe that Zr/Al, in contrast to its correlation with Pa/Th, is only loosely connected with our εNd values and K/Ti ratio, which track deep-water provenance (Fig. 5). The different εNd and K/Ti fingerprints during the strong AMOC interval of MIS 5 and MIS 1 (Fig. 5), suggests that (i) changes in deep-water provenance alone did not determine the position or strength of the DWBC with additional processes such as LSW production and advection likely playing significant roles, and (ii) proxies of the physical position of the DWBC in the water column, such as Zr/Al ratios, might provide reliable insights into past changes in the AMOC.

6.2. *Deep-water variability in the outer Labrador Sea during the past 550,000 years*

Utilizing the insights from the data encompassing the past ca. 140 kyr, we now extend the interpretation of our proxy records to encompass the past ca. 550 kyr (Fig. 6). Consistent with the last climatic cycle, we observe a tight linkage between εNd and K/Ti variability across the past 550 kyr. However, this linkage does not conform to a systematic glacial-interglacial pattern.

Beginning with the glacial conditions, we find that except for the peak of MIS 10, all other glacial peaks of MIS 6, 8, and 12) follow the LGM (MIS 2) pattern characterized by relatively radiogenic εNd signatures (median: -17 ± 2) and enriched Ti-rich detrital deposition (Fig. 6). In contrast, the signature of the MIS 10 peak more closely resembles that of MIS 5 with median εNd values of -20 ± 2 and higher K-concentrations. This suggests that during the LGM, along with most glacial peak conditions of the past ca. 550 kyr, Ti-rich detritus was transported to the study site by an active DWBC receiving contributions from Nordic Sea overflow water. This finding corroborates earlier studies indicating the existence of an active DWBC fed by Nordic Sea overflow water during the past 400 kyr (Blaser et al., 2020; Fagel et al., 1996, 1997, 1999; Fagel and Hillaire-Marcel, 2006; Stevenard et al., 2024). The continuous flux of Ti-rich detritus to our study site via the DWBC suggests persistent erosion and washout cycles from regions containing source rocks the Paleogene Volcanic Province. These cycles likely coincide with the waxing and waning of regional ice sheets. The less radiogenic εNd signatures alongside the increased K/Ti values observed during the peak of MIS 10, compared to other peaks of glacial stages, could be attributed to smaller ice sheet coverage across the Hudson Bay-Superior Provenance terrane region during this period. This

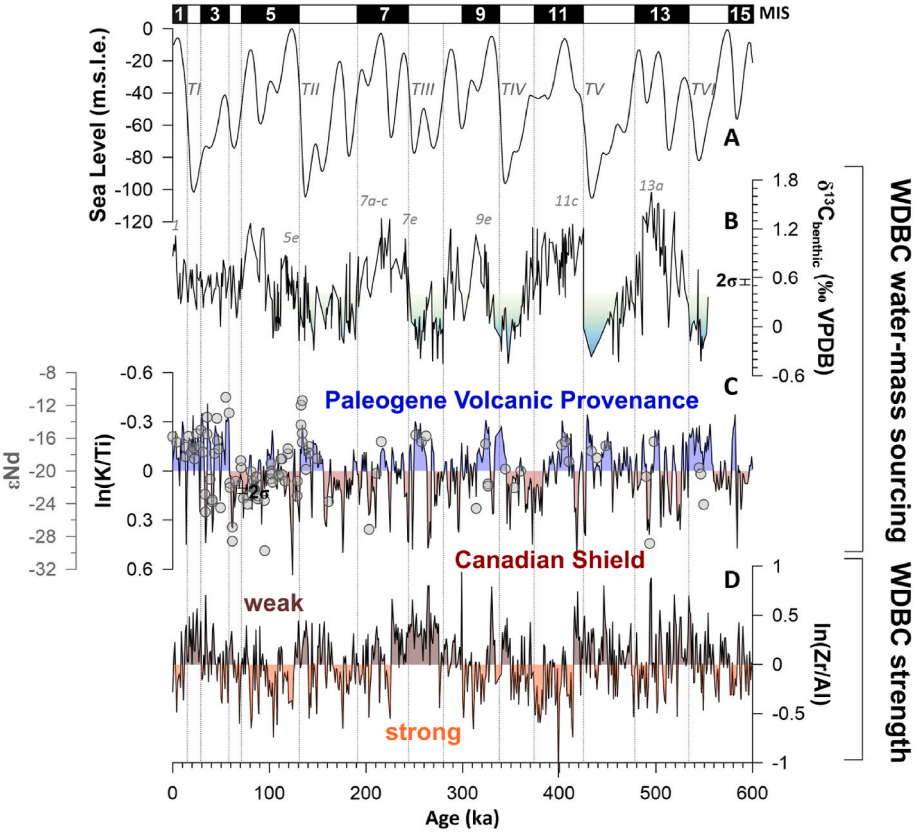

Fig. 6. Evolution of Deep Western Boundary Current (DWBC) during the past ~550 kyr. (**A**) Sea level in meters with respect to present-day (m.s.l.e) following Stap et al. (2016); (**B**) composite benthic stable carbon isotope ($\delta^{13}C_b$) record of Site U1302/03; (**C**) detrended and linearly resampled (~1 kyr step size) ln(K/Ti) ratio with the superimposed composite εNd isotope record (grey dots) of Site U1302/03 (this study); (**D**) detrended and linearly resampled (~1 kyr step size) ln(Zr/Al) ratio of Site U1302/03 (this study). Assignment of Marine Isotope stages (MIS) and terminations (T) follows Lisiecki and Raymo (2005).

scenario might have led to a higher detrital material supply into and from the inner Labrador Sea to our study site, potentially augmented by enhanced Labrador Current strength. Model simulations of Laurentide Ice Sheet extent across the past ca. 800 kyr suggest that MIS 10 peak conditions had the lowest LIS extent compared to MIS 2, 6, 8, and 12 (Batchelor et al., 2019). The only other colder climatic phases comparable in terms of ice sheet extent to MIS 10 might have been MIS 4 and most likely MIS 14 (Batchelor et al., 2019), as also highlighted by similar εNd values (median: -20 ± 2) and K-enriched deposition (Fig. 6). In terms of DWBC strength, we find that all peak glacial periods are characterized by a coarsening of the sediment, implying a shallowing of the DWBC regardless of the prevailing deep-water mass provenance.

Moving on to interglacial stages, MIS 11, including 11c, exhibits the most similar characteristics to MIS 1 in its εNd and K/Ti imprint (Fig. 6), thus resembling modern conditions with where overflow water from the Nordic Seas significantly contributing to the DWBC. In contrast, MIS 7, 9, and 13, including 9e and 13a, follow the εNd and K/Ti pattern of MIS 5, including 5e. This suggests increased contributions of Labrador Sea-based detritus to our study site, likely driven by a combination of factors (i) increased weathering intensities delivering circum-Labrador Sea detritus to the inner Labrador Sea in association with (ii) an enhanced Labrador Current detritus, and/or (iii) reduced overflow water mass contributions to the DWBC. In terms of DWBC strength, during the interglacial periods of MIS 1, 5e, 9e, 11c and 13a a fining of the sediment in line with a strong DWBC can be observed, while Zr/A data from MIS 7e signals weakened DWBC strength. These findings from our Zr/Al data actually corroborate previous arguments about interglacial AMOC variability during the past 550 kyr, which that highlight that in particular MIS 7 was characterized by a reduced AMOC strength (Bouttes et al., 2020).

Lastly, we compared our Zr/Al, K/Ti, and εNd data with our $\delta^{13}C_b$ record across the past ca. 550 kyr (Fig. 6). The $\delta^{13}C_b$ ratio is often used as an indicator of ocean circulation patterns, as ocean circulation (i.e., stratification) is a key factor determining oceanic $\delta^{13}C_b$ distribution (Duplessy et al., 1988). Generally, phases of decreased bottom-water $\delta^{13}C$ in the deep North Atlantic correlate with weakened AMOC phases, and *vice versa*. We observe that phases of increased fine sediment deposition correspond to increased $\delta^{13}C_b$ values at our site, while coarser sediment phases correspond to decreased $\delta^{13}C_b$ values (Fig. 6). However, $\delta^{13}C_b$ values across similar phases of finer sediment deposition can vary by up to 0.8 ‰ (e.g., MIS 1 $\delta^{13}C_b = 1.2$ ‰ vs. MIS 5e $\delta^{13}C_b = 0.4$ ‰; Fig. 6), while coarser grain sediment intervals exhibit $\delta^{13}C_b$ signatures ranging between 0.6 ‰ (LGM) and −0.2 ‰ (peak MIS 12; Fig. 6). This complexity may be attributed to various factors, including the utilization of multi-benthic foraminifera species for reconstruction of $\delta^{13}C_b$ as it is the case here. Specifically, *U. peregrina* has been argued to record $\delta^{13}C$ of an infaunal habitat that is offset from $\delta^{13}C$ of the overlying bottom water (Gottschalk et al., 2016). However, comparing our $\delta^{13}C_b$ record with the predominately-*C. wuellerstorfi* derived $\delta^{13}C_b$ record of Site U1308 (see Supplementary Fig. S4; Hodell et al., 2008; Hodell and Channell, 2016) reveals a close correlation ($r = 0.6$; $p < 0.001$), suggesting that the potential bias introduced by including shallow infaunal *U. peregrina* in our analyses is minimal. Hence, the discrepancies observed between $\delta^{13}C_b$, Zr/Al, and εNd (see Supplementary Fig. S3) imply diverse and independent driving mechanisms for each of these proxies. In the case of $\delta^{13}C_b$, it has been suggested that variability in the mid-latitudinal North Atlantic was strongly influenced by the remineralization of organic matter and/or changes in air-sea carbon exchange (Bouttes et al., 2020; Broecker and Maier-Reimer, 1992; Lynch-Stieglitz et al., 2007; Pöppelmeier et al., 2021, 2022).

To summarize, based on these findings, we argue that an active DWBC was likely a persistent feature within the Labrador Sea region throughout the past 550 kyr (Fig. 6). Our study demonstrates that the glacial/interglacial pattern in DWBC strength reported in earlier studies prevailed throughout this whole interval. Glacial stages were characterized by a shallower DWBC, while interglacial stages, with the exception of MIS 7e, all suggest an enhanced DWBC.

Additionally, the dominant deep-water masses feeding into the DWBC during glacial-interglacial periods varied frequently from regional (K-rich, unradiogenic εNd) to more distal sources in the Nordic Seas (Ti-rich, radiogenic εNd).

7. Conclusions

In conclusion, our study aimed to investigate changes in the deep-water regime of the outer Labrador Sea region over the past 550 kyr, focusing on deep-water provenance and circulation strength during glacial-interglacial cycles. Utilizing a combination of geochemical proxies, including benthic foraminiferal stable isotopes, neodymium isotopes, and XRF-scanning-based elemental ratios from IODP Sites U1302/03, we have gained new insights into the dynamics of deep-water circulation in this area.

Our findings suggest that an active DWBC persistently influenced the outer Labrador Sea region throughout the past 550 kyr. While peak glacial periods exhibited a weakened or shoaled DWBC, most interglacial periods indicated a deeper and strengthened DWBC. Interestingly, the dominant deep-water masses feeding into the DWBC during glacial and interglacial periods varied from regional (K-rich, unradiogenic εNd) to more distal sources in the Nordic Seas (Ti-rich, radiogenic εNd). However, these changes in deep-water provenance did not consistently correlate with DWBC strength, suggesting that additional factors may have played a significant role in shaping the DWBC.

Our results also highlight potential limitations in commonly used proxies for deep-water mass and circulation strength, underscoring the necessity for further multi-proxy studies in complex deep-water settings such as the outer Labrador Sea. By gaining a better understanding of the sensitive interplay between deep-water mass source changes and Atlantic Meridional Overturning Circulation strength on geological timescales, we can enhance our insights into the mechanisms driving climate variability in the North Atlantic region.

CRediT authorship contribution statement

Stefanie Kaboth-Bahr: Writing – review & editing, Writing – original draft, Visualization, Validation, Investigation, Funding acquisition, Formal analysis, Data curation, Conceptualization. **André Bahr:** Writing – review & editing, Writing – original draft. **Patrick Blaser:** Writing – review & editing, Writing – original draft, Methodology, Funding acquisition, Formal analysis, Data curation. **Antje H.L. Voelker:** Writing – review & editing, Writing – original draft. **Jörg Lippold:** Writing – review & editing, Methodology, Investigation. **Marcus Gutjahr:** Investigation, Methodology, Writing – review & editing. **David A. Hodell:** Writing – review & editing, Data curation. **James E.T. Channell:** Writing – review & editing, Data curation. **Anne de Vernal:** Writing – review & editing, Writing – original draft, Investigation, Funding acquisition, Conceptualization. **Claude Hillaire-Marcel:** Writing – review & editing, Writing – original draft, Methodology, Funding acquisition, Data curation, Conceptualization.

Declaration of competing interest

The authors declare that they have no known competing financial interests or personal relationships that could have appeared to influence the work reported in this paper.

Acknowledgements

SKB acknowledges funding from ECORD Young Scientist Grant as well as an Open-Top Post-Doc fellowship of the University of Potsdam. AHLV received Portuguese national funds from FCT - Foundation for Science and Technology through projects UIDB/04326/2020, UIDP/04326/2020 and LA/P/0101/2020. PB acknowledges funding by the

European Union's Horizon Europe research and innovation program (grant agreement ID 101065424, project OxyQuant).

Appendix A. Supplementary data

Supplementary data to this article can be found online at https://doi.org/10.1016/j.qsa.2025.100266.

Data availability

All the data presented in this study can be found at.https://doi.pangaea.de/10.1594/PANGAEA.949491.

References

Atamanchuk, D., Koelling, J., Send, U., Wallace, D.W.R., 2020. Rapid transfer of oxygen to the deep ocean mediated by bubbles. Nat. Geosci. 13, 232–237. https://doi.org/10.1038/s41561-020-0532-2.

Bahr, A., Jiménez-Espejo, F.J., Kolasinac, N., Grunert, P., Hernández-Molina, F.J., Röhl, U., Voelker, A.H.L., Escutia, C., Stow, D.A.V., Hodell, D., Alvarez-Zarikian, C. A., 2014. Deciphering bottom current velocity and paleoclimate signals from contourite deposits in the Gulf of Cadiz during the last 140kyr: an inorganic geochemical approach. Geochem. Geophys. Geosyst. 15, 3145–3160. https://doi.org/10.1002/2014GC005356.

Ballini, M., Kissel, C., Colin, C., Richter, T., 2006. Deep-water mass source and dynamic associated with rapid climatic variations during the last glacial stage in the North Atlantic: a multiproxy investigation of the detrital fraction of deep-sea sediments. Geochem. Geophys. Geosyst. 7, Q02N01. https://doi.org/10.1029/2005GC001070.

Batchelor, C.L., Margold, M., Krapp, M., Murton, D.K., Dalton, A.S., Gibbard, P.L., Stokes, C.R., Murton, J.B., Manica, A., 2019. The configuration of Northern Hemisphere ice sheets through the Quaternary. Nat. Commun. 10, 3713. https://doi.org/10.1038/s41467-019-11601-2.

Biscaye, P.E., 1965. Mineralogy and sedimentation of recent deep-sea clay in the Atlantic Ocean and adjacent seas and oceans. Bull. Geol. Soc. Am. 76, 803–831. https://doi.org/10.1130/0016-7606(1965)76[803:MASORD]2.0.CO;2.

Blaser, P., Gutjahr, M., Pöppelmeier, F., Frank, M., Kaboth-Bahr, S., Lippold, J., 2020. Labrador Sea bottom water provenance and REE exchange during the past 35,000 years. Earth Planet Sci. Lett. 542, 116299. https://doi.org/10.1016/j.epsl.2020.116299.

Blaser, P., Lippold, J., Gutjahr, M., Frank, N., Link, J.M., Frank, M., 2016. Extracting foraminiferal seawater Nd isotope signatures from bulk deep sea sediment by chemical leaching. Chem. Geol. 439, 189–204. https://doi.org/10.1016/j.chemgeo.2016.06.024.

Böhm, E., Lippold, J., Gutjahr, M., Frank, M., Blaser, P., Antz, B., Fohlmeister, J., Frank, N., Andersen, M.B., Deininger, M., 2015. Strong and deep Atlantic meridional overturning circulation during the last glacial cycle. Nature 517, 73–76. https://doi.org/10.1038/nature14059.

Bouttes, N., Vazquez Riveiros, N., Govin, A., Swingedouw, D., Sanchez-Goni, M.F., Crosta, X., Roche, D.M., 2020. Carbon 13 isotopes reveal limited ocean circulation changes between interglacials of the last 800 ka. Paleoceanogr. Paleoclimatol. 35, PA003776. https://doi.org/10.1029/2019PA003776.

Bower, A.S., Lozier, M.S., Gary, S.F., Böning, C.W., 2009. Interior pathways of the North Atlantic meridional overturning circulation. Nature 459, 243–247. https://doi.org/10.1038/nature07979.

Box, G.E.P., Jenkins, G.M., Reinsel, G.C., Ljung, G.M., 2015. Time Series Analysis: Forecating and Control, fifth ed. Wiley-Blackwell.

Boyer, T.P., Antonov, J.I., Baranova, O.K., Coleman, C., Garcia, H.E., Grodsky, A., Johnson, D.R., Locarnini, R.A., Mishonov, A.V., O'Brien, T.D., 2013. World Ocean Database 2013, vol. 73. NOAA Atlas NESDIS.

Brambilla, E., Talley, L.D., 2008. Subpolar mode water in the northeastern Atlantic: 1. Averaged properties and mean circulation. J. Geophys. Res. Ocean. 113, JC004062. https://doi.org/10.1029/2006JC004062.

Brambilla, E., Talley, L.D., Robbins, P.E., 2008. Subpolar mode water in the northeastern Atlantic: 2. Origin and transformation. J. Geophys. Res. Ocean. 113, C04026. https://doi.org/10.1029/2006JC004063.

Broecker, W.S., Maier-Reimer, E., 1992. The influence of air and sea exchange on the carbon isotope distribution in the sea. Global Biogeochem. Cycles 6, 315–320. https://doi.org/10.1029/92GB01672.

Bryden, H.L., Longworth, H.R., Cunningham, S.A., 2005. Slowing of the Atlantic meridional overturning circulation at 25° N. Nature 438, 655–657. https://doi.org/10.1038/nature04385.

Burckel, P., Waelbroeck, C., Luo, Y., Roche, D.M., Pichat, S., Jaccard, S.L., Gherardi, J., Govin, A., Lippold, J., Thil, F., 2016. Changes in the geometry and strength of the Atlantic meridional overturning circulation during the last glacial (20–50 ka). Clim. Past 12, 2061–2075. https://doi.org/10.5194/cp-12-2061-2016.

Burkholder, K.C., Lozier, M.S., 2014. Tracing the pathways of the upper limb of the North atlantic meridional overturning circulation. Geophys. Res. Lett. 41, 4254–4260. https://doi.org/10.1002/2014GL060226.

Caesar, L., McCarthy, G.D., Thornalley, D.J.R., Cahill, N., Rahmstorf, S., 2021. Current atlantic meridional overturning circulation weakest in last millennium. Nat. Geosci. 14, 118–120. https://doi.org/10.1038/s41561-021-00699-z.

Caesar, L., Rahmstorf, S., Robinson, A., Feulner, G., Saba, V., 2018. Observed fingerprint of a weakening Atlantic Ocean overturning circulation. Nature 556, 191–196. https://doi.org/10.1038/s41586-018-0006-5.

Chalk, T.B., Hain, M.P., Foster, G.L., Rohling, E.J., Sexton, P.F., Badger, M.P.S., Cherry, S. G., Hasenfratz, A.P., Haug, G.H., Jaccard, S.L., Martínez-García, A., Pälike, H., Pancost, R.D., Wilson, P.A., 2017. Causes of ice age intensification across the Mid-Pleistocene Transition. Proc. Natl. Acad. Sci. USA 115, 13114–13119. https://doi.org/10.1073/pnas.1702143114.

Channell, J.E.T., Hodell, D.A., Romero, O., Hillaire-Marcel, C., de Vernal, A., Stoner, J.S., Mazaud, A., Röhl, U., 2012. A 750-kyr detrital-layer stratigraphy for the North atlantic (IODP sites U1302–U1303, orphan Knoll, Labrador Sea). Earth Planet Sci. Lett. 317–318, 218–230. https://doi.org/10.1016/j.epsl.2011.11.029.

Channell, J.E.T., Kanamatsu, T., Sato, T., Stein, R., Alvarez-Zarikian, C.A., Malone, M.J., the Expedition 303/306 Scientists, 2006. North atlantic climate expeditions 303 and 306 of the riserless drilling platform from st. John's, Newfoundland (Canada), to ponta delgada, azores (Portugal) sites U1302–U1308 25 september–17 november 2004 and from ponta delgada, azores (Portugal), to dub. Integr. Ocean Drill. Progr. Manag. Int. Inc., Integr. Ocean Drill. Progr. https://doi.org/10.2204/iodp.proc.303306.214.2010.

Channell, J.E.T., Wright, J.D., Mazaud, A., Stoner, J.S., 2014. Age through tandem correlation of Quaternary relative paleointensity (RPI) and oxygen isotope data at IODP Site U1306 (Eirik Drift, SW Greenland). Quat. Sci. Rev. 88, 135–146. https://doi.org/10.1016/j.quascirev.2014.01.022.

Channell, J.E.T., Xuan, C., Hodell, D.A., 2009. Stacking paleointensity and oxygen isotope data for the last 1.5 Myr (PISO-1500). Earth Planet Sci. Lett. 283, 14–23. https://doi.org/10.1016/j.epsl.2009.03.012.

Crocket, K.C., Vance, D., Foster, G.L., Richards, D.A., Tranter, M., 2012. Continental weathering fluxes during the last glacial/interglacial cycle: insights from the marine sedimentary Pb isotope record at Orphan Knoll, NW Atlantic. Quat. Sci. Rev. 38, 89–99. https://doi.org/10.1016/j.quascirev.2012.02.004.

Curry, W.B., Oppo, D.W., 2005. Glacial water mass geometry and the distribution of $\delta^{13}C$ of ΣCO_2 in the western Atlantic Ocean. Paleoceanography 20, PA001021. https://doi.org/10.1029/2004PA001021.

Davies, S., Stow, D., Nicholson, U., 2021. Late Glacial to Holocene sedimentary facies of the Eirik Drift, southern Greenland margin: spatial and temporal variability and paleoceanographic implications. Mar. Geol. 440, 106568. https://doi.org/10.1016/j.margeo.2021.106568.

Dickson, R.R., Brown, J., 1994. The production of North Atlantic Deep Water: sources, rates, and pathways. J. Geophys. Res. 99, 12319–12341. https://doi.org/10.1029/94jc00530.

Duplessy, J.C., Shackleton, N.J., Fairbanks, R.G., Labeyrie, L., Oppo, D., Kallel, N., 1988. Deepwater source variations during the last climatic cycle and their impact on the global deepwater circulation. Paleoceanography 3, 343–360. https://doi.org/10.1029/PA003i003p00343.

Fagel, N., Hillaire-Marcel, C., 2006. Glacial/interglacial instabilities of the Western Boundary under Current during the last 365 kyr from Sm/Nd ratios of the sedimentary clay-size fractions at ODP site 646 (Labrador Sea). Mar. Geol. 232, 87–99. https://doi.org/10.1016/j.margeo.2006.08.006.

Fagel, N., Hillaire-Marcel, C., Robert, C., 1997. Changes in the western boundary undercurrent outflow since the last glacial maximum, from smectite/illite ratios in deep Labrador Sea sediments. Paleoceanography 12, 79–96. https://doi.org/10.1029/96PA02877.

Fagel, N., Innocent, C., Stevenson, R.K., Hillaire-Marcel, C., 1999. Deep circulation changes in the Labrador Sea since the last glacial maximum: new constraints from Sm-Nd data on sediments. Paleoceanography 14, 777–788. https://doi.org/10.1029/1999PA900041.

Fagel, N., Robert, C., Hillaire-Marcel, C., 1996. Clay mineral signature of the NW atlantic boundary undercurrent. Mar. Geol. 130, 19–28. https://doi.org/10.1016/0025-3227(95)00134-4.

Fagel, N., Robert, C., Preda, M., Thorez, J., 2001. Smectite composition as a tracer of deep circulation: the case of the Northern North Atlantic. Mar. Geol. 172, 309–330. https://doi.org/10.1016/S0025-3227(00)00123-7.

Filippova, A., Frank, M., Kienast, M., Gutjahr, M., Hathorne, E.C., Hillaire-Marcel, C., 2023. Authigenic and detrital carbonate Nd isotope records reflect pulses of detrital material input to the Labrador Sea during the Heinrich stadials. Paleoceanogr. Paleoclimatol. 38, e2022PA004470. https://doi.org/10.1029/2022PA004470.

Filippova, A., Frank, M., Kienast, M., Rickli, J., Hathorne, E., Yashayaev, I.M., Pahnke, K., 2017. Water mass circulation and weathering inputs in the Labrador Sea based on coupled Hf–Nd isotope compositions and rare earth element distributions. GCA 199, 164–184. https://doi.org/10.1016/j.gca.2016.11.024.

Foukal, N.P., Lozier, M.S., 2016. No inter-gyre pathway for sea-surface temperature anomalies in the North Atlantic. Nat. Commun. 7, 11333. https://doi.org/10.1038/ncomms11333.

Frank, M., 2002. Radiogenic isotopes: tracers of past ocean circulation and erosional input. Rev. Geophys. 40, G000094. https://doi.org/10.1029/2000RG000094.

Frew, R.D., Dennis, P.F., Heywood, K.J., Meredith, M.P., Boswell, S.M., 2000. The oxygen isotope composition of water masses in the northern North Atlantic. Deep. Res. Part I Oceanogr. Res. Pap. 47, 2265–2286. https://doi.org/10.1016/S0967-0637(00)00023-6.

Fu, Y., Feili, L., Karstensen, J., Wang, C., 2020. A stable atlantic meridional overturning circulation in a changing North Atlantic ocean since the 1990s. Sci. Adv. 6, eabc7836. https://doi.org/10.1126/sciadv.abc7836.

Galaasen, E.V., Ninnemann, U.S., Kessler, A., Irvalı, N., Rosenthal, Y., Tjiputra, J., Bouttes, N., Roche, D.M., Kleiven, H.F., Hodell, D.A., 2020. Interglacial instability of North Atlantic deep water ventilation. Science 367, 1485–1489. https://doi.org/10.1126/science.aay6381.

García-Ibáñez, M.I., Pardo, P.C., Carracedo, L.I., Mercier, H., Lherminier, P., Ríos, A.F., Pérez, F.F., 2015. Structure, transports and transformations of the water masses in the Atlantic Subpolar Gyre. Prog. Oceanogr. 135, 18–36. https://doi.org/10.1016/j.pocean.2015.03.009.

Gebbie, G., 2014. How much did glacial North Atlantic water shoal? Paleoceanography 29, 190–209. https://doi.org/10.1002/2013PA002557.

Gonzales, M.V., De Almeida, F.K., Costa, K.B., Santarosa, A.C.A., Camillo, E., De Quadros, J.P., Toledo, F.A.L., 2017. Help index: hoeglundina elegans preservation index for marine sediments in the western South Atlantic. J. Foraminifer. Res. 47, 56–69. https://doi.org/10.2113/gsjfr.47.1.56.

Gottschalk, J., Vázquez Riveiros, N., Waelbroeck, C., Skinner, L.C., Michel, E., Duplessy, J.C., Hodell, D., Mackensen, A., 2016. Carbon isotope offsets between benthic foraminifer species of the genus *Cibicides* (*Cibicidoides*) in the glacial sub-Antarctic Atlantic. Paleoceanography 31, 1583–1602. https://doi.org/10.1002/2016PA003029.

Griffin, J.J., Windom, H., Goldberg, E.D., 1968. The distribution of clay minerals in the World Ocean. Deep. Res. Oceanogr. Abstr. 15, 433–459. https://doi.org/10.1016/0011-7471(68)90051-X.

Grousset, F., Latouche, C., Parra, M., 1982. Late quaternary sedimentation between the gibbs fracture and the Greenland basin: mineralogical and geochemical data. Mar. Geol. 47, 303–330. https://doi.org/10.1016/0025-3227(82)90074-3.

Grützner, J., Higgins, S.M., 2010. Threshold behavior of millennial scale variability in deep water hydrography inferred from a 1.1 Ma long record of sediment provenance at the southern Gardar Drift. Paleoceanography 25, PA4204. https://doi.org/10.1029/2009PA001873.

Haley, B.A., Du, J., Abbott, A.N., McManus, J., 2017. The impact of benthic processes on rare earth element and neodymium isotope distributions in the oceans. Front. Mar. Sci. 4, 426. https://doi.org/10.3389/fmars.2017.00426.

Handmann, P., Fischer, J., Visbeck, M., Karstensen, J., Biastoch, A., Böning, C., Patara, L., 2018. The deep western boundary current in the Labrador Sea from observations and a high-resolution model. J. Geophys. Res. Ocean. 123, JC013702. https://doi.org/10.1002/2017JC013702.

Hasenfratz, A.P., Jaccard, S.L., Martínez-García, A., Sigman, D.M., Hodell, D.A., Vance, D., Bernasconi, S.M., Kleiven, H.F., Haumann, F.A., Haug, G.H., 2019. The residence time of Southern Ocean surface waters and the 100,000-year ice age cycle. Science 363, 1080–1084. https://doi.org/10.1126/science.aat7067.

Hillaire-Marcel, C., de Vernal, A., McKay, J., 2011. Foraminifer isotope study of the Pleistocene Labrador Sea, northwest North Atlantic (IODP Sites 1302/03 and 1305), with emphasis on paleoceanographical differences between its "inner" and "outer" basins. Mar. Geol. 279, 188–198. https://doi.org/10.1016/j.margeo.2010.11.001.

Hillaire-Marcel, C., de Vernal, A., Bilodeau, G., Weaver, A.J., 2001. Absence of deep-water formation in the Labrador Sea during the last interglacial period. Nature 410, 1073–1077. https://doi.org/10.1038/35074059.

Hillaire-Marcel, C., Maccali, J., Menabreaz, L., Ghaleb, B., Poirier, A., Edinger, E., 2022. U-Series ages and neodymium isotopic compositions of late quaternary populations of Desmophyllum dianthus from orphan Knoll and flemish cap. South-eastern Labrador Sea. PANGAEA. https://doi.org/10.1594/PANGAEA.949618.

Hodell, D.A., Channell, J.E.T., 2016. Mode transitions in Northern Hemisphere glaciation: co-evolution of millennial and orbital variability in Quaternary climate. Clim. Past 12, 1805–1828. https://doi.org/10.5194/cp-12-1805-2016.

Hodell, D.A., Channell, J.E.T., Curtis, J.H., Romero, O.E., Röhl, U., 2008. Onset of "Hudson strait'' Heinrich eventsin the eastern North Atlantic at the end of the middle Pleistocene transition (~640ka)? Paleoceanography 23, PA4218. https://doi.org/10.1029/2008PA001591.

Hodell, D.A., Crowhurst, S.J., Lourens, L., Margari, V., Nicolson, J., Rolfe, J.E., Skinner, L.C., Thomas, N.C., Tzedakis, P.C., Mleneck-Vautravers, M.J., Wolff, E.W., 2023. A 1.5-million-year record of orbital and millennial climate variability in the North Atlantic. Clim. Past 19, 607–636. https://doi.org/10.5194/cp-19-607-2023.

Hodell, D.A., Evans, H.F., Channell, J.E.T., Curtis, J.H., 2010. Phase relationships of North Atlantic ice-rafted debris and surface-deep climate proxies during the last glacial period. Quat. Sci. Rev. 29, 3875–3886. https://doi.org/10.1016/j.quascirev.2010.09.006.

Hoffmann, S.S., Dalsing, R.E., Murphy, S.C., 2019. Sortable silt records of intermediate-depth circulation and sedimentation in the southwest Labrador Sea since the last glacial maximum. Quat. Sci. Rev. 206, 99–110. https://doi.org/10.1016/j.quascirev.2018.12.028.

Hönisch, B., Hemming, N.G., Archer, D., Siddall, M., McManus, J.F., 2009. Atmospheric carbon dioxide concentration across the Mid-Pleistocene transition. Science 324, 1551–1554. https://doi.org/10.1126/science.1171477.

Howe, J.N.W., Piotrowski, A.M., 2017. Atlantic deep water provenance decoupled from atmospheric CO_2 concentration during the lukewarm interglacials. Nat. Commun. 8, 2003. https://doi.org/10.1038/s41467-017-01939-w.

Howe, J.N.W., Piotrowski, A.M., Noble, T.L., Mulitza, S., Chiessi, C.M., Bayon, G., 2016. North atlantic deep water production during the last glacial maximum. Nat. Commun. 7, 11765. https://doi.org/10.1038/ncomms11765.

Hunter, S., Wilkinson, D., Louarn, E., McCave, I.N., Rohling, E., Stow, D.A., Bacon, S., 2007. Deep western boundary current dynamics and associated sedimentation on the Eirik Drift, Southern Greenland Margin. Deep-Sea Res. I: Oceanogr. Res. Pap. 54, 2036–2066. https://doi.org/10.1016/j.dsr.2007.09.007.

IPCC, 2021. AR6 Climate Change 2021: the Physical Science Basis, Contribution of Working Group I to the Sixth Assessment Report of the Intergovernmental Panel on Climate Change.

Jeandel, C., 2016. Overview of the mechanisms that could explain the "Boundary Exchange" at the land-ocean contact. Philos. Trans. R. Soc. A Math. Phys. Eng. Sci. 374, 20150287. https://doi.org/10.1098/rsta.2015.0287.

Kawase, M., Sarmiento, J.J., 1986. Circulation and nutrients in mid-depth Atlantic waters. J. Geophys. Res. 91, 9749–9770.

Keigwin, L.D., Swift, S.A., 2017. Carbon isotope evidence for a northern source of deep water in the glacial western North Atlantic. Proc. Natl. Acad. Sci. U.S.A. 114, 2831–2835. https://doi.org/10.1073/pnas.1614693114.

Kieke, D., Rhein, M., Stramma, L., Smethie, W.M., Bullister, J.L., LeBel, D.A., 2007. Changes in the pool of labrador Sea Water in the subpolar North Atlantic. Geophys. Res. Lett. 34, L06605. https://doi.org/10.1029/2006GL028959.

Kilbourne, K.H., Wanamaker, A.D., Moffa-Sanchez, P., Reynolds, D.J., Amrhein, D.E., Butler, P.G., Gebbie, G., Goes, M., Jansen, M.F., Little, C.M., Mette, M., Moreno-Chamarro, E., Ortega, P., Otto-Bliesner, B.L., Rossby, T., Scourse, J., Whitney, N.M., 2022. Atlantic circulation change still uncertain. Nat. Geosci. 15, 165–167. https://doi.org/10.1038/s41561-022-00896-4.

Kissel, C., Laj, C., Labeyrie, L., Dokken, T., Voelker, A., Blamart, D., 1999. Rapid climatic variations during marine isotopic stage 3: magnetic analysis of sediments from Nordic Seas and North Atlantic. Earth Planet Sci. Lett. 171, 489–502. https://doi.org/10.1016/S0012-821X(99)00162-4.

Knies, J., Vogt, C., Stein, R., 1998. Late Quaternary growth and decay of the Svalbard/Barents Sea ice sheet and paleoceanographic evolution in the adjacent Arctic Ocean. Geo Mar. Lett. 18, 195–202. https://doi.org/10.1007/s003670050068.

Lackschewitz, K.S., Wallrabe-Adams, H.J., Garbe-Schönberg, D., 1994. Geochemistry of surface sediments from the mid-oceanic kolbeinsey ridge, north of Iceland. Mar. Geol. 121, 105–119. https://doi.org/10.1016/0025-3227(94)90160-0.

Lacan, F., Jeandel, C., 2005. Neodymium isotopes as a new tool for quantifying exchange fluxes at the continent–ocean interface. Earth Planet Sci. Lett. 232, 245–257. https://doi.org/10.1016/j.epsl.2005.01.004.

Lavrov, V.M., Nikolayeva, V.K., Barash, M.S., 1971. Titanium in the quaternary deposits of the Atlantic Ocean. Oceanology 13, 57–62.

Lee, A., Ellet, D.J., 1967. Recirculating components to the deep boundary current of the northern North Atlantic. Deep Sea Res. 14, 183–190.

Lippold, J., Gutjahr, M., Blaser, P., Christner, E., Ferreira, M.-L.C., Mulitza, S., Christl, M., Wombacher, F., Böhm, E., Antz, B., Cartapanis, O., Vogel, H., Jaccard, S., 2016. Deep water provenance and dynamics of the (de)glacial Atlantic meridional overturning circulation. Earth Planet Sci. Lett. 445, 68–78. https://doi.org/10.1016/j.epsl.2016.04.013.

Lippold, J., Pöppelmeier, F., Süfke, F., Gutjahr, M., Goepfert, T.J., Blaser, P., Friedrich, O., Link, J.M., Wacker, L., Rheinberger, S., Jaccard, S.L., 2019. Constraining the variability of the atlantic meridional overturning circulation during the Holocene. Geophys. Res. Lett. 46, 11338–11346. https://doi.org/10.1029/2019GL084988.

Lisiecki, L.E., Raymo, M.E., 2005. A Pliocene-Pleistocene stack of 57 globally distributed benthic $\delta^{18}O$ records. Paleoceanography 20, 1–17. https://doi.org/10.1029/2004PA001071.

Lozier, M.S., 2010. Deconstructing the conveyor belt. Science 328, 1507–1511. https://doi.org/10.1126/science.1189250.

Lozier, M.S., Gary, S.F., Bower, A.S., 2013. Simulated pathways of the overflow waters in the North Atlantic: subpolar to subtropical export. Deep. Res. Part II Top. Stud. Oceanogr. 85, 147–153. https://doi.org/10.1016/j.dsr2.2012.07.037.

Lozier, M.S., Li, F., Bacon, S., Bahr, F., Bower, A.S., Cunningham, S.A., De Jong, M.F., De Steur, L., DeYoung, B., Fischer, J., Gary, S.F., Greenan, B.J.W., Holliday, N.P., Houk, A., Houpert, L., Inall, M.E., Johns, W.E., Johnson, H.L., Johnson, C., Karstensen, J., Koman, G., Le Bras, I.A., Lin, X., Mackay, N., Marshall, D.P., Mercier, H., Oltmanns, M., Pickart, R.S., Ramsey, A.L., Rayner, D., Straneo, F., Thierry, V., Torres, D.J., Williams, R.G., Wilson, C., Yang, J., Yashayaev, I., Zhao, J., 2019. A sea change in our view of overturning in the subpolar North Atlantic. Science 363, 516–521. https://doi.org/10.1126/science.aau6592.

Lynch-Stieglitz, J., Adkins, J.F., Curry, W.B., Dokken, T., Hall, I.R., Herguera, J.C., Hirschi, J.J.M., Ivanova, E.V., Kissel, C., Marchal, O., Marchitto, T.M., McCave, I.N., McManus, J.F., Mulitza, S., Ninnemann, U., Peeters, F., Yu, E.F., Zahn, R., 2007. Atlantic meridional overturning circulation during the last glacial maximum. Science 316, 66–69. https://doi.org/10.1126/science.1137127.

Maccali, J., Hillaire-Marcel, C., Ménabréaz, L., Ghaleb, B., Blénet, A., Edinger, E., Hélie, J.F., Preda, M., 2020. Late Quaternary sporadic development of Desmophyllum dianthus deep-coral populations in the southern Labrador Sea with specific attention to their ^{14}C- and ^{230}Th-dating. Mar. Chem. 224, 103807. https://doi.org/10.1016/j.marchem.2020.103807.

Marshall, J., Schott, F., 1999. Open-ocean convection: observations, theory, and models. Rev. Geophys. 37, 1–64. https://doi.org/10.1029/98RG02739.

McCartney, M.S., 1992. Recirculating components to the deep boundary current of the northern North Atlantic. Prog. Oceanogr. 29, 283–383. https://doi.org/10.1016/0079-6611(92)90006-L.

McCartney, M.S., Talley, L.D., 1982. The subpolar mode water of the North Atlantic Ocean. J. Phys. Oceanogr. 12, 1169–1188. https://doi.org/10.1175/1520-0485(1982)012<1169:tsmwot>2.0.co;2.

McCave, I.N., Thornalley, D.J.R., Hall, I.R., 2017. Relation of sortable silt grain-size to deep-sea current speeds: calibration of the 'Mud Current Meter. ' Deep. Res. Part I Oceanogr. Res. Pap. 127, 1–12. https://doi.org/10.1016/j.dsr.2017.07.003.

McCorkle, D.C., Corliss, B.H., Farnham, C.A., 1997. Vertical distributions and stable isotopic compositions of live (stained) benthic foraminifera from the North Carolina and California continental margins. Deep. Res. Part I Oceanogr. Res. Pap. 44, 983–1024. https://doi.org/10.1016/S0967-0637(97)00004-6.

McManus, J.F., Oppo, D.W., Cullen, J.L., 1999. A 0.5-million-year record of millennial-scale climate variability in the North atlantic. Science 283, 971–975. https://doi.org/10.1126/science.283.5404.971.

Mertens, C., Rhein, M., Walter, M., Böning, C.W., Behrens, E., Kieke, D., Steinfeldt, R., Stöber, U., 2014. Circulation and transports in the Newfoundland basin, western

subpolar North Atlantic. J. Geophys. Res.: Oceans 119, 7772–7793. https://doi.org/10.1002/2014JC010019.
Meyers, S.R., 2014. Astrochron: an R Package for Astrochronology.
Molinari, R.L., Fine, R.A., Douglas Wilson, W., Curry, R.G., Abell, J., McCartney, M.S., 1998. The arrival of recently formed Labrador Sea Water in the deep western boundary current at 26.5 °N. Geophys. Res. Lett. 25, 2249–2252. https://doi.org/10.1029/98GL01853.
Müller-Michaelis, A., Uenzelmann-Neben, G., 2014. Development of the western boundary undercurrent at Eirik Drift related to changing climate since the early Miocene. Deep-Sea Res. Part A Oceanogr. Res. Pap. 93, 21–34. https://doi.org/10.1016/j.dsr.2014.07.010.
Nees, S., Struck, U., 1999. Benthic foraminiferal response to major paleoceanographic changes. In: Abrantes, F., Mix, A.C. (Eds.), Reconstructing Ocean History: A Window into the Future. Springer, US, Boston, MA, pp. 195–216. https://doi.org/10.1007/978-1-4615-4197-4_13.
Nichols, M.D., Xuan, C., Crowhurst, S., Hodell, D.A., Richter, C., Acton, G.D., Wilson, P. A., 2020. Climate-induced variability in mediterranean outflow to the North Atlantic Ocean during the late Pleistocene. Paleoceanogr. Paleoclimatol. 35, e2020PA003947. https://doi.org/10.1029/2020PA003947.
Oppo, D.W., Gebbie, G., Huang, K.-F., Curry, W.B., Marchitto, T.M., Pietro, K.R., 2018. Data constraints on glacial atlantic water mass geometry and properties. Paleoceanogr. Paleoclimatol. 33, 1013–1034. https://doi.org/10.1029/2018PA003408.
Pacini, A., Pickart, R.S., 2022. Meanders of the West Greenland current near cape farewell. Deep. Res. Part I Oceanogr. Res. Pap. 179, 103664. https://doi.org/10.1016/j.dsr.2021.103664.
Parker, R.L., Foster, G.L., Gutjahr, M., Wilson, P.A., Littler, K.L., Cooper, M.J., Michalik, A., Milton, J.A., Crocket, K.C., Bailey, I., 2022. Laurentide Ice Sheet extent over the last 130 thousand years traced by the Pb isotope signature of weathering inputs to the Labrador Sea. Quat. Sci. Rev. 287, 107564. https://doi.org/10.1016/j.quascirev.2022.107564.
Parra, M., Puechmaille, C., Dumon, J.C., Delmont, P., Ferragne, A., 1986. Geochemistry of Tertiary alterite clay phases on the Iceland-Faeroe Ridge (northeast Atlantic), leg 38, site 336. Chem. Geol. 54, 165–176. https://doi.org/10.1016/0009-2541(86)90081-1.
Pena, L.D., Goldstein, S.L., 2014. Thermohaline circulation crisis and impacts during the mid-Pleistocene transition. Science 345, 318–322. https://doi.org/10.1126/science.1249770.
Pickart, R.S., Straneo, F., Moore, G.W.K., 2003. Is labrador Sea Water formed in the Irminger Basin? Deep. Res. Part I Oceanogr. Res. Pap. 50, 23–52. https://doi.org/10.1016/S0967-0637(02)00134-6.
Piotrowski, A.M., Goldstein, S.L., Hemming, S.R., Fairbanks, R.G., 2004. Intensification and variability of ocean thermohaline circulation through the last deglaciation. Earth Planet Sci. Lett. 225, 205–220. https://doi.org/10.1016/j.epsl.2004.06.002.
Pöppelmeier, F., Blaser, P., Gutjahr, M., Jaccard, S.L., Frank, M., Max, L., Lippold, J., 2020. Northern-sourced water dominated the Atlantic Ocean during the last glacial maximum. Geology 48, 826–829. https://doi.org/10.1130/G47628.1.
Pöppelmeier, F., Blaser, P., Gutjahr, M., Süfke, F., Thornalley, D.J.R., Grützner, J., Jakob, K.A., Link, J.M., Szidat, S., Lippold, J., 2019. Influence of ocean circulation and benthic exchange on deep Northwest Atlantic Nd isotope records during the past 30,000 Years. Geochem. Geophys. Geosyst. 20, GC008271. https://doi.org/10.1029/2019GC008271.
Pöppelmeier, F., Gutjahr, M., Blaser, P., Schulz, H., Süfke, F., Lippold, J., 2021. Stable Atlantic deep water mass sourcing on glacial-interglacial timescales. Geophys. Res. Lett. 48, GL092722. https://doi.org/10.1029/2021GL092722.
Pöppelmeier, F., Lippold, J., Blaser, P., Gutjahr, M., Frank, M., Stocker, T.F., 2022. Neodymium isotopes as a paleo-water mass tracer: a model-data reassessment. Quat. Sci. Rev. 279, 107404. https://doi.org/10.1016/j.quascirev.2022.107404.
Praetorius, S.K., McManus, J.F., Oppo, D.W., Curry, W.B., 2008. Episodic reductions in bottom-water currents since the last ice age. Nat. Geosci. 1, 449–452. https://doi.org/10.1038/ngeo227.
Rashid, H., Piper, D.J., Drapeau, J., Marin, C., Smith, M.E., 2019. Sedimentology and history of sediment sources to the NW Labrador Sea during the past glacial cycle. Quat. Sci. Rev. 221, 105880. https://doi.org/10.1016/j.quascirev.2019.105880.
Rasmussen, T.L., Thomsen, E., 2004. The role of the North Atlantic Drift in the millennial timescale glacial climate fluctuations. Palaeogeogr. Palaeoclimatol. Palaeoecol. 210, 101–116. https://doi.org/10.1016/j.palaeo.2004.04.005.
Sarnthein, M., Winn, K., Jung, S.J.A., Duplessy, J.-C., Labeyrie, L., Erlenkeuser, H., Ganssen, G., 1994. Changes in east atlantic deepwater circulation over the last 30,000 years: eight time slice reconstructions. Paleoceanography 9, 209–267. https://doi.org/10.1029/93PA03301.
Schlitzer, R., 2002. Interactive analysis and visualization of geoscience data with Ocean Data View. Comput. Geosci. 28, 1211–1218. https://doi.org/10.1016/S0098-3004(02)00040-7.
Schönfeld, J., Altenbach, A.V., 2005. Late Glacial to Recent distribution pattern of deep-water Uvigerina species in the north-eastern Atlantic. Mar. Micropaleontol. 57, 1–24. https://doi.org/10.1016/j.marmicro.2005.05.004.
Seidenkrantz, M.S., Kuijpers, A., Aagaard-Sørensen, S., Lindgreen, H., Olsen, J., Pearce, C., 2021. Evidence for influx of atlantic water masses to the Labrador Sea during the last glacial maximum. Sci. Rep. 11, 6788. https://doi.org/10.1038/s41598-021-86224-z.
Shackleton, N.J., Hall, M.A., 1984. Oxygen and carbon isotope stratigraphy of the deep sea drilling project hole 552A: Plio-Pleistocene glacial history. Initial Reports DSDP 81, 599–609.
Spielhagen, R., 2004. Arctic Ocean deep-sea record of northern Eurasian ice sheet history. Quat. Sci. Rev. 23, 1455–1483. https://doi.org/10.1016/j.quascirev.2003.12.015.
Stap, L.B., de Boer, B., Ziegler, M., Bintanja, R., Lourens, L.J., van de Wal, R.S., 2016. CO_2 over the past 5 million years: continuous simulation and new δ^{11}B-based proxy data. Earth Planet Sci. Lett. 439, 1–10. https://doi.org/10.1016/j.epsl.2016.01.022.
Stevenard, N., Kissel, C., Govin, A., Wandres, C., 2024. Deep North Atlantic circulation strength: glacial-interglacial variability over the last 400,000 years. Quat. Sci. Rev. 345, 109011. https://doi.org/10.1016/j.quascirev.2024.109011.
Streeter, S.S., Lavery, S.A., 1982. Holocene and latest glacial benthic foraminifera from the slope and rise off eastern North America. Geol. Soc. Am. Bull. 93, 190–199. https://doi.org/10.1130/0016-7606(1982)93<190:HALGBF>2.0.CO;2.
Struve, T., Roberts, N.L., Frank, M., Piotrowski, A.M., Spielhagen, R.F., Gutjahr, M., Teschner, C., Bauch, H.A., 2019. Ice-sheet driven weathering input and water mass mixing in the Nordic Seas during the last 25,000 years. Earth Planet Sci. Lett. 514, 108–118. https://doi.org/10.1016/j.epsl.2019.02.030.
Struve, T., van de Flierdt, T., Burke, A., Robinson, L.F., Hammond, S.J., Crocket, K.C., Bradtmiller, L.I., Auro, M.E., Mohamed, K.J., White, N.J., 2017. Neodymium isotopes and concentrations in aragonitic scleractinian cold-water coral skeletons - modern calibration and evaluation of palaeo-applications. Chem. Geol. 453, 148–168. https://doi.org/10.1016/j.chemgeo.2017.01.022.
Sy, A., Rheint, M., Lazier, J.R.N., Koltermann, K.P., Meincke, J., Putzka, A., Bersch, M., 1997. Surprisingly rapid spreading of newly formed intermediate waters across the North Atlantic Ocean. Nature. https://doi.org/10.1038/386675a0.
Tanaka, T., Togashi, S., Kamioka, H., Amakawa, H., Kagami, H., Hamamoto, T., Yuhara, M., Orihashi, Y., Yoneda, S., Shimizu, H., Kunimaru, T., Takahashi, K., Yanagi, T., Nakano, T., Fujimaki, H., Shinjo, R., Asahara, Y., Tanimizu, M., Dragusanu, C., 2000. JNdi-1: a neodymium isotopic reference in consistency with LaJolla neodymium. Chem. Geol. 168, 279–281. https://doi.org/10.1016/S0009-2541(00)00198-4.
Tanhua, T., Olsson, K.A., Jeansson, E., 2005. Formation of Denmark Strait overflow water and its hydro-chemical composition. J. Mar. Syst. 57, 264–268. https://doi.org/10.1016/j.jmarsys.2005.05.003.
Thornalley, D.J.R., Blaschek, M., Davies, F.J., Praetorius, S., Oppo, D.W., McManus, J.F., Hall, I.R., Kleiven, H., Renssen, H., McCave, I.N., 2013. Long-term variations in Iceland-Scotland overflow strength during the Holocene. Clim. Past 9, 2073–2084. https://doi.org/10.5194/cp-9-2073-2013.
Thornalley, D.J.R., Elderfield, H., McCave, I.N., 2010. Intermediate and deep water paleoceanography of the northern North Atlantic over the past 21,000 years. Paleoceanography 25, PA001833. https://doi.org/10.1029/2009PA001833.
Vidal, L., Labeyrie, L., Cortijo, E., Arnold, M., Duplessy, J.C., Michel, E., Becqué, S., Van Weering, T.C.E., 1997. Evidence for changes in the North atlantic deep water linked to meltwater surges during the Heinrich events. Earth Planet Sci. Lett. 146, 13–27. https://doi.org/10.1016/s0012-821x(96)00192-6.
Vogt, C., Knies, J., 2008. Sediment dynamics in the Eurasian Arctic Ocean during the last deglaciation - the clay mineral group smectite perspective. Mar. Geol. 250, 211–222. https://doi.org/10.1016/j.margeo.2008.01.006.
Watkins, S.J., Maher, B.A., 2003. Magnetic characterisation of present-day deep-sea sediments and sources in the North Atlantic. Earth Planet Sci. Lett. 214, 379–394. https://doi.org/10.1016/S0012-821X(03)00422-9.
Weltje, G.J., Bloemsma, M.R., Tjallingii, R., Heslop, D., Röhl, U., Croudace, I.W., 2015. Prediction of geochemical composition from XRF core scanner data: a new multivariate approach including automatic selection of calibration samples and quantification of uncertainties. In: Micro-XRF Studies of Sediment Cores. Springer, Amsterdam.
Yang, Q., Dixon, T.H., Myers, P.G., Bonin, J., Chambers, D., Van Den Broeke, M.R., 2016. Recent increases in Arctic freshwater flux affects Labrador Sea convection and Atlantic overturning circulation. Nat. Commun. 7, 10525. https://doi.org/10.1038/ncomms10525.
Yang, Y., Piper, D.J.W., 2021. Alongflow variability of the labrador current during the Holocene. Quat. Sci. Rev. 267, 107110. https://doi.org/10.1016/j.quascirev.2021.107110.
Yashayaev, I., van Aken, H.M., Holliday, N.P., Bersch, M., 2007. Transformation of the labrador Sea water in the subpolar North Atlantic. Geophys. Res. Lett. 34, L22605. https://doi.org/10.1029/2007GL031812.
Yu, J., Elderfield, H., Piotrowski, A.M., 2008. Seawater carbonate ion-δ^{13}C systematics and application to glacial-interglacial North Atlantic Ocean circulation. Earth Planet Sci. Lett. 271, 209–220. https://doi.org/10.1016/j.epsl.2008.04.010.
Zhao, N., Oppo, D.W., Huang, K.F., Howe, J.N.W., Blusztajn, J., Keigwin, L.D., 2019. Glacial interglacial Nd isotope variability of North Atlantic Deep Water modulated by North American ice sheet. Nat. Commun. 10, 1e10. https://doi.org/10.1038/s41467-019-13707-z.F.
Zimmermann, H.B., 1982. Fine-grained sediment distribution in the late pleistocene/holocene North Atlantic. Bull. Inst. Geol. Bassin Aquitaine 31, 337–357.